JOURNAL OF GEOPHYSICAL RESEARCH, VOL. 113, B11401, doi:10.1029/2007JB005002, 2008

Effective stress and pore pressure in the Nankai accretionary prism off the Muroto Peninsula, southwestern Japan

Takeshi Tsuji,[1,2] Hidekazu Tokuyama,[1] Patrizia Costa Pisani,[3] and Gregory Moore[4]

Received 20 February 2007; revised 11 July 2008; accepted 15 August 2008; published 4 November 2008.

[1] We developed a theoretical method for predicting effective stress and pore pressure based on rock physics model. We applied the method to reveal the pore pressure distribution within the Nankai accretionary prism off southwestern Japan and to investigate variations in pore pressure associated with evolution of the plate boundary décollement. From the crack aspect ratio spectrum estimated from laboratory and well-log data, we calculated a theoretical relationship between acoustic velocity and mean effective stress by using differential effective medium theory. By iteratively fitting the theoretically calculated velocity to the seismic velocities derived from 3D tomographic inversion, we estimated in situ mean effective stress within the accretionary prism. Pore pressure is then the difference between the effective stress and the confining stress. When we calculated pore pressure, we considered compressive state of stress in the accretionary prism. Our results confirm that pore fluid pressure is high within the subducting sedimentary sequence below the décollement; we determined a normalized pore pressure ratio (λ^*) of 0.4–0.7. Abnormal pore pressures develop in the underthrust sequence as a result of the increase in overburden load because of the thickened overlying prism and a low permeability barrier across the décollement. Overpressuring within the accreted sequence is initiated at the deformation front and proceeds landward. The increase in horizontal compaction within the accreted sequence may raise pore pressures within the accreted sequence, and the pore pressure (mean effective stress) contrast at the décollement becomes smaller landward of the deformation front.

Citation: Tsuji, T., H. Tokuyama, P. Costa Pisani, and G. Moore (2008), Effective stress and pore pressure in the Nankai accretionary prism off the Muroto Peninsula, southwestern Japan, *J. Geophys. Res.*, *113*, B11401, doi:10.1029/2007JB005002.

1. Introduction

[2] Characterization of pore fluid pressures at plate boundary décollements (detachments that separate a deforming accretionary prism from the underthrusting sediments) is critical for understanding the strength and structural development of décollements, and the taper angle of accretionary prisms [*Davis et al.*, 1983; *Dahlen*, 1984; *Hubbert and Rubey*, 1959]. In addition, because high pore pressure near the décollement decreases the effective stress, the development of abnormal pore pressures influences the position of the shallow limit of seismogenic faulting [e.g., *Moore and Saffer*, 2001; *Scholz*, 1998]. Several studies [e.g., *Screaton et al.*, 2002; *Straub*, 2002; *Saffer*, 2003] have successfully estimated pore fluid pressures at drill sites that have penetrated the décollement of the Nankai accretionary prism.

[3] Seismic reflection data have shown that the décollement characteristics of the Nankai and Barbados accretionary prisms can be recognized on the basis of their reflection polarities, seismic velocities, and other seismic attributes [e.g., *Moore and Shipley*, 1993; *Shipley et al.*, 1994; *Bangs et al.*, 1996, 1999, 2004; *Zhao et al.*, 2000; *Tsuji et al.*, 2005a]. These studies using seismic data have focused mainly on the décollement reflection only in order to reveal its characteristics including pore pressure, although some studies have used seismic velocity data to predict pore pressure distributions within some accretionary wedges: the Nankai accretionary prism [*Tobin and Saffer*, 2003], the Barbados accretionary prism [*Westbrook*, 1991; *Hayward et al.*, 2003], and the Oregon accretionary prism [*Cochrane et al.*, 1994].

[4] Many previous studies of pore pressure prediction from seismic interval velocities have relied on empirical relationships [e.g., *Eaton*, 1972; *Han and Nur*, 1986; *Eberhart-Phillips and Han*, 1989; *Dutta*, 2001]. If the sedimentary sequence is stratified and many boreholes penetrate it, it is relatively easy to estimate pore pressure by comparing an abnormal compaction trend with a normal compaction trend or by assuming a compaction disequilibrium regime [e.g., *Rubey and Hubbert*, 1959; *Eaton*, 1972]. However, because few boreholes penetrate the Nankai accretionary prism, which becomes progressively more

[1]Ocean Research Institute, University of Tokyo, Tokyo, Japan.
[2]Now at Department of Civil and Earth Resources Engineering, Kyoto University, Kyoto, Japan.
[3]Customer Support Asia-Pacific, Paradigm Geophysical, Perth, Australia.
[4]Department of Geology and Geophysics, University of Hawaii, Hawaii, USA.

0148-0227/08/2007JB005002$09.00

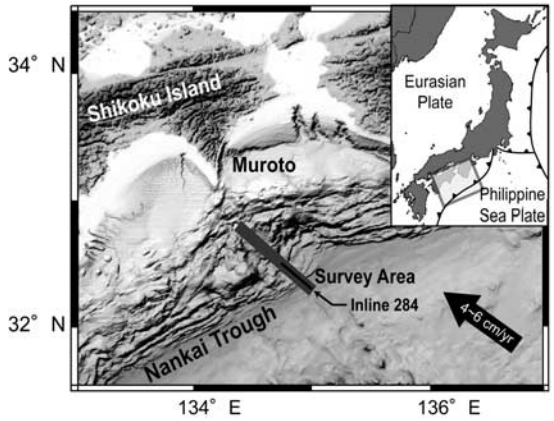

Figure 1. Bathymetric image of the Nankai Trough showing the 3-D seismic survey area (gray rectangle). Inline 284 (xlines 400–1600), which was used for pore pressure prediction in this study, is shown as a black line.

consolidated and cemented in the landward direction [e.g., *Taira et al.*, 1991; *Moore et al.*, 2001b; *Mikada et al.*, 2002; *Morgan et al.*, 2007], it is difficult to define appropriate normal compaction trends. Furthermore, high-pressure fluid intervention due to clay dehydration [*Powers*, 1959] or fluid migration [e.g., *von Huene and Lee*, 1982] decreases seismic velocities without much change in porosity, because these unloading procedures open thin cracks of low porosity and softens grain-to-grain contacts [e.g., *Kuster and Toksoz*, 1974]. Therefore it is difficult to predict pore pressure in the deeper parts of the décollement. Instead of using normal compaction trends or assuming a compaction disequilibrium regime, we need to predict pore pressure by using an estimated relationship between velocity and effective stress. Here, we predict effective stress and pore fluid pressure within the Nankai accretionary prism off the Muroto Peninsula by applying rock physics theory to conditioned seismic interval velocities. In this theoretical method, we predict effective stress and pore pressure distribution from velocity–stress relationships by using laboratory-derived data on the relationship between *P* wave and *S* wave velocities and effective stress.

[5] Many theoretical models have been proposed that attempt to establish a link between formation parameters and velocities [e.g., *Mavko et al.*, 1998]. The relationship between effective stress and velocity depends on pore volume, pore shape, mineral texture, and mineral composition [e.g., *Schon*, 2004]. Total porosity (pore volume) is one of the most important parameters of those that constrain velocities [e.g., *Hyndman et al.*, 1993]. However, pore shape (e.g., crack or void) also significantly influences seismic velocity, independent of total porosity. Because thin cracks with small pore volume can significantly decrease velocities [*Kuster and Toksoz*, 1974], we need to consider pore features other than total porosity. To construct velocity–stress relationships that can be used to predict pore pressures therefore we need to consider pore geometries (e.g., aspect ratio). For unconsolidated shallow sedimentary sequences close to the seafloor, seismic velocities increase with effective stress as a result of the strengthening of grain contacts as effective stress increases [*Mindlin*, 1949; *Dvorkin and Nur*, 1996]. In consolidated rocks, closure of cracks in the rock in response to increasing effective stress is the main influence on velocity [e.g., *Kuster and Toksoz*, 1974; *Carcione et al.*, 2003]. Because we mainly focused on pore pressure in relatively consolidated sediments near the décollement, we used an effective-medium crack-inclusion model [e.g., *Kuster and Toksoz*, 1974; *Norris*, 1985; *Berryman*, 1992]. We introduce an application of the aspect ratio spectrum of pore space [e.g., *Toksoz et al.*, 1976; *Cheng and Toksoz*, 1979] and Differential Effective Medium (DEM) theory [e.g., *Berryman*, 1992] to predict effective stress and pore pressure from seismic reflection data.

2. Geologic Setting

[6] The Nankai Trough is at a plate convergent margin where the Philippine Sea plate is subducting beneath southwestern Japan (Figure 1). The rate of subduction is 4–6 cm/yr on an azimuth of 310°–315° [*Seno et al.*, 1993; *Ito et al.*, 1999; *Miyazaki and Heki*, 2001]. This subduction zone has repeatedly generated great earthquakes with magnitudes greater than Mw 8 [*Ando*, 1975]. Our study area off the Muroto Peninsula of Shikoku Island shows high heat flow [*Yamano et al.*, 2003], because it is located near the extension of the extinct Shikoku Basin back-arc spreading ridge (Kinan Seamounts), which ceased spreading at 15 Ma [*Okino et al.*, 1999].

[7] The plate boundary décollement in the Nankai Trough off the Muroto Peninsula is developed within a hemipelagic mudstone sequence (lower Shikoku facies) [*Taira et al.*, 1991] and it is well defined by a prominent reverse-polarity reflector on seismic profiles (Figure 2) [*Moore et al.*, 1990]. On the basis of this polarity reversal, the décollement in our survey area is inferred to be a zone of low acoustic impedance. Because the décollement is within a relatively homogeneous mudstone sequence, the low acoustic impedance in the underthrust sequence can be explained by high porosity sustained by high pore pressure (compaction disequilibrium) [e.g., *Moore et al.*, 2001a], or by the expansion of thin cracks as a result of unloading due to fluid intervention, as inferred for the Oregon and Barbados accretionary prisms [e.g., *Cochrane et al.*, 1994; *Bangs et al.*, 1999]. The abnormal high pore fluid pressure, which is far higher than hydrostatic pressure, accounts for the weak coupling along the décollement and the low taper angle of the accretionary prism off the Muroto Peninsula [e.g., *Hubbert and Rubey*, 1959; *Davis et al.*, 1983].

3. Data set

3.1. Seismic Interval Velocity

[8] The 3-D multichannel seismic reflection data (Figure 2a), acquired by the *R/V Ewing* in 1999 [e.g., *Moore et al.*, 2001a], was processed to estimate seismic interval (*P* wave) velocities within the accretionary prism. The 80 km × 8 km survey area comprised 81 individual lines with cross-track spacing of ~100 m. Because of streamer feathering due to the strong Kuroshio Current [*Tsuji et al.*, 2005b], the total width in the crossline direction was effectively 9 km. The azimuth of individual lines was ~314°, which is nearly parallel to the direction of subduction of the Philippine Sea plate. The survey employed

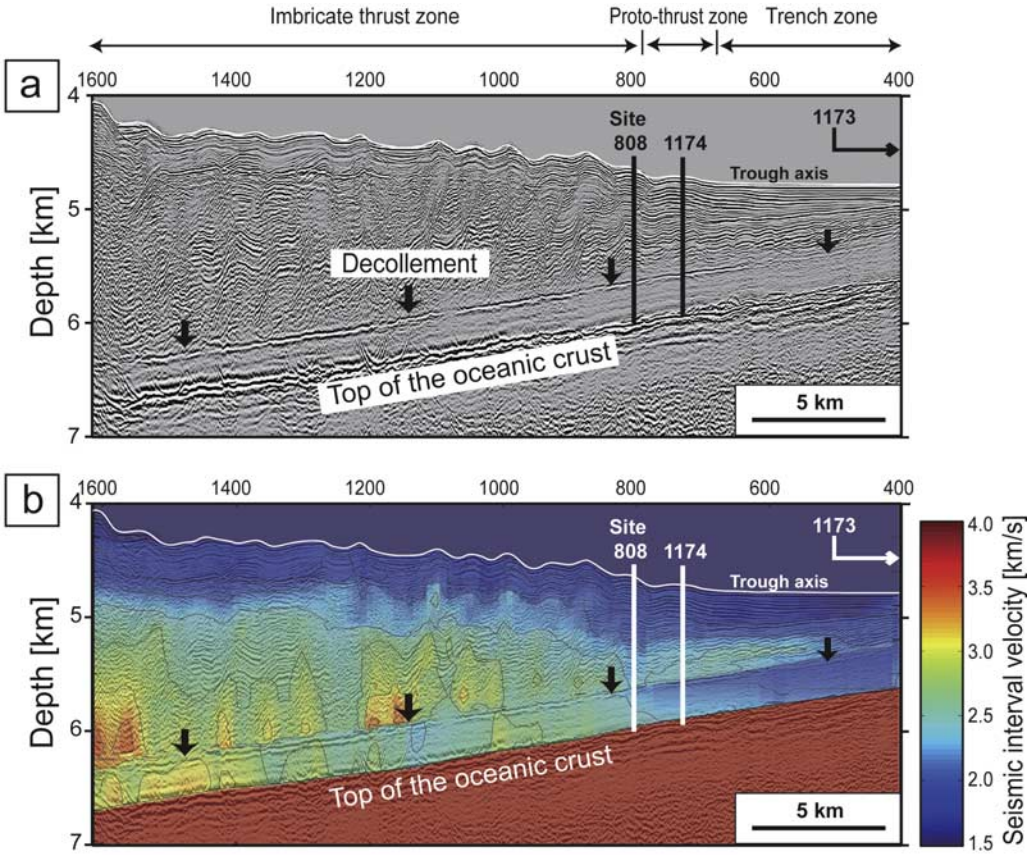

Figure 2. (a) Seismic profile across the Nankai Trough (inline 284, xlines 400–1600) showing locations of ODP sites and the interpreted décollement. The numbers above the profile represent xline common mid point numbers. (b) Seismic interval velocity obtained by 3-D reflection tomography [*Costa Pisani et al.*, 2005]. The contours on this profile represent interval velocity every 300 m/s. Velocity within the oceanic crust was not determined.

a source array of 14 air guns with a total volume of 70 L (4276 in^3) fired at 50-m intervals. A 240-channel, 6-km-long streamer cable was used, and the recording time for each shot was 12 seconds. The bin size for 3-D seismic data processing was 25 m in the inline direction and 50 m in the crossline direction [*Moore et al.*, 2001a; *Bangs et al.*, 2004].

[9] Pore pressure prediction requires high-resolution interval velocities obtained by seismic inversion techniques [e.g., *Sayers et al.*, 2002; *Dutta*, 2001; *Carcione et al.*, 2003]. We used a seismic interval velocity volume that was assembled by running iterative horizon-based tomography, prestack depth migration, and residual moveout corrections (Figure 2b) [*Yilmaz and Doherty*, 2001; *Costa Pisani et al.*, 2005]. This velocity model flattens the gathers and provides good quality images that resolve the complex structure of the Nankai Trough. Initial mismatches between the seismic data (velocities and depths) and borehole data were minimized or eliminated by tying the depth of the key horizons in the seismic sections to those at drill sites [*Costa Pisani et al.*, 2005]. This involved performing a geologically consistent velocity analysis following stratigraphic and structural boundaries. We used an unsmoothed version of the seismic velocity volume to avoid losing resolution of the real high-frequency velocity variations related to geological layering (Figure 2b). This procedure provided a final 3-D interval velocity volume that closely resembles the rock velocities and can therefore be used for pore pressure prediction.

[10] To delineate the pressure distribution in the subduction direction of the Philippine Sea plate, we extracted the 2-D velocity model of inline 284, which is perpendicular to the trough axis and crosses Ocean Drilling Program (ODP) Sites 808 and 1174 (Figure 2b). Channel and patchy structures along the décollement that were observed at the Barbados décollement [*Shipley et al.*, 1994; *Moore et al.*, 1998; *Bangs et al.*, 1999; *Zhao et al.*, 2000] were not clearly evident in our survey data [*Bangs et al.*, 2004; *Tsuji et al.*, 2005a]. Furthermore, we did not find a clear velocity change in the crossline direction. Therefore we believe that a 2-D velocity model (inline direction) is sufficiently accurate to reveal the pore pressure distribution at the front of the accretionary prism. The velocity variations over short distances observed above the décollement (Figure 2b) may be artifacts due to the short streamer offset used and the complex structure above this zone.

[11] We chose to use the seaward part of the 3-D survey data (crosslines 400–1600; Figure 2) because the accuracy of the velocities determined from seismic data decreases in the landward direction (as the décollement becomes deeper) and the effect of thermal alteration on the elastic moduli of sediment grains increases. Our study area covers the Shikoku Basin (trench zone), the proto-thrust zone, and the imbricate

thrust zone (Figure 2). The proto-thrust zone begins at the deformation front, where detachment and growth of the accretionary prism is initiated. The imbricate thrust zone consists of a series of well-developed imbricate packages spaced several kilometers apart. The décollement steps down to the surface of the oceanic crust further landward (outside) of our study area [*Bangs et al.*, 2004].

3.2. Borehole Data (ODP Sites 1173, 1174, and 808)

[12] ODP Sites 1174 and 808 are within the study area (Figure 2). Site 1173 is a reference site, ~11 km seaward of the trough axis, and is considered to be in a hydrostatic state. The décollement, penetrated at Site 1174 between 808 and 840 m below seafloor (mbsf), was identified by fractures and brecciation in the lower Shikoku facies. Site 808 was drilled ~3 km landward of the deformation front. The décollement at Site 808 was identified by intense brittle deformation at 945 to 964 mbsf, and deformation was observed to be greater than that at Site 1174 [*Taira et al.*, 1991; *Moore et al.*, 2001b]. Unfortunately, no holes were drilled landward of the frontal thrust region.

[13] Well-log data were acquired at Sites 1173 and 808 [*Mikada et al.*, 2002], and core samples were obtained at Sites 1173, 1174, and 808 [*Taira et al.*, 1991; *Moore et al.*, 2001b]. We used mainly the physical properties from the well-log data for pore pressure prediction because the well-log data should represent the in situ values from the borehole. In this study, the borehole parameters we used were *P* wave velocity, porosity, density, and the mineral components. Because well-logs were not obtained at Site 1174 or from the underthrust sequence at Site 808, we used properties measured later in discrete subsurface samples at atmospheric (rather than downhole) pressure. *Hoffman and Tobin* [2004] defined the mean difference between the porosity measured from core samples and well-log porosity at Site 1173, which we applied to the porosities of the core samples to account for the lower (surface) pressures at which these porosities were measured [*Mikada et al.*, 2002; *Hoffman and Tobin*, 2004].

[14] To estimate grain elastic moduli (K_0 and μ_0) in the boreholes, we used the mineral components present (clay, quartz, plagioclase, and calcite), as estimated from X-ray diffraction (XRD) analyses of randomly oriented bulk-sediment powders from Sites 1173 and 1174 [*Shipboard Scientific Party*, 2001a, 2001b]. There are three possible ways to calculate the elastic moduli of mixtures of minerals: these are by using the Voigt, Reuss, or Hill average [e.g., *Hill*, 1952; *Mavko et al.*, 1998; *Avseth et al.*, 2005]. Here, the grain elastic moduli of mixtures of clay, quartz, plagioclase, and calcite were estimated by using the Voigt higher average equation, because the final results (pressure distribution) estimated using the Voigt equation are similar to those estimated by the Hill or Reuss equations. The elastic modulus of each mineral was obtained from *Mavko et al.* [1998].

[15] The grain elastic moduli within the accretionary prism were then estimated by extrapolating the mineralogy at Site 1174 in both the seaward and landward directions. Although the diagenetic boundary between the upper and lower Shikoku facies is obvious at Site 1173 [e.g., *Spinelli et al.*, 2007] and ambiguous at Site 1174, the overall mineralogical fractions at Sites 1173 and 1174 are similar. Therefore the above extrapolation of mineralogy should be reliable. Furthermore, we used only the seaward part of the 3-D seismic survey area for our analysis (Figure 2) and assumed that grain elastic moduli do not change laterally within this area.

3.3. Laboratory-Derived Velocities

[16] Because the acoustic velocities of the core samples from Sites 1173, 1174, and 808 were not measured under confining stresses, we measured the velocities of outcrop samples from the Nobeoka thrust in Kyushu, southwestern Japan [*Tsuji et al.*, 2006], and of seafloor outcrop samples obtained from the Nankai accretionary prism off the Kii Peninsula by the Japan Agency for Marine-Earth Science and Technology (JAMSTEC) submersible vessel *Shinkai 6500*. Although these samples were different from those of our study area, they do come from the Nankai accretionary prism. Therefore we used their acoustic properties for pore pressure prediction. The core samples analyzed were ~3.8 cm wide and 2.5–5.0 cm long. We used the pulse transmission technique, with a principal frequency of 500 kHz, to determine *P* wave and *S* wave velocities. Travel times were measured after digitizing each trace at 6250 points at a time sweep of $\sim 5 \times 10^{-5}$ s.

3.3.1. Nobeoka Outcrop Samples

[17] The Nobeoka thrust is interpreted to be a fossil seismogenic mega-splay fault, and its original structure is still preserved [*Kondo et al.*, 2005; *Okamoto et al.*, 2006]. Although in this study we assumed cracks in the rocks to be randomly oriented such that they do not contribute to velocity anisotropy, the samples drilled from the hanging wall of Nobeoka thrust exhibit velocity anisotropy due to a foliation [*Tsuji et al.*, 2006]. Therefore we used only weakly foliated samples drilled from the footwall of the thrust. The measured porosity of the Nobeoka outcrop samples was <7%, which suggests that they are more consolidated than the décollement rocks of our study area (10–30% porosity).

[18] For the low-porosity Nobeoka outcrop samples, *P* wave and *S* wave velocities were measured under dry conditions (Figure 3a), because fluid dispersion masks pressure effects under saturated conditions and because the low permeability of the samples prevented the generation of pore fluid pressure [*Tsuji et al.*, 2006]. *P* wave and *S* wave velocities increase with increasing effective stress mainly as a result of compaction and closure of micro-cracks and flaws, and increased contact between grain boundaries [e.g., *Kuster and Toksoz*, 1974].

3.3.2. Seafloor Outcrop Samples

[19] Several samples were obtained by the *Shinkai 6500* (YK0602 and YK0603) from the submarine canyon and the seafloor trace of the seismogenic mega-splay fault (*Omine* ridge). The porosities of these samples were relatively high (15–43%). Their velocities were measured under saturated conditions (Figure 3b). To obtain velocities of totally saturated samples, we applied pore fluid pressure in addition to the confining stress before the measurements. Furthermore, because the seafloor outcrop samples shorten under effective stress, vertical linear variable differential

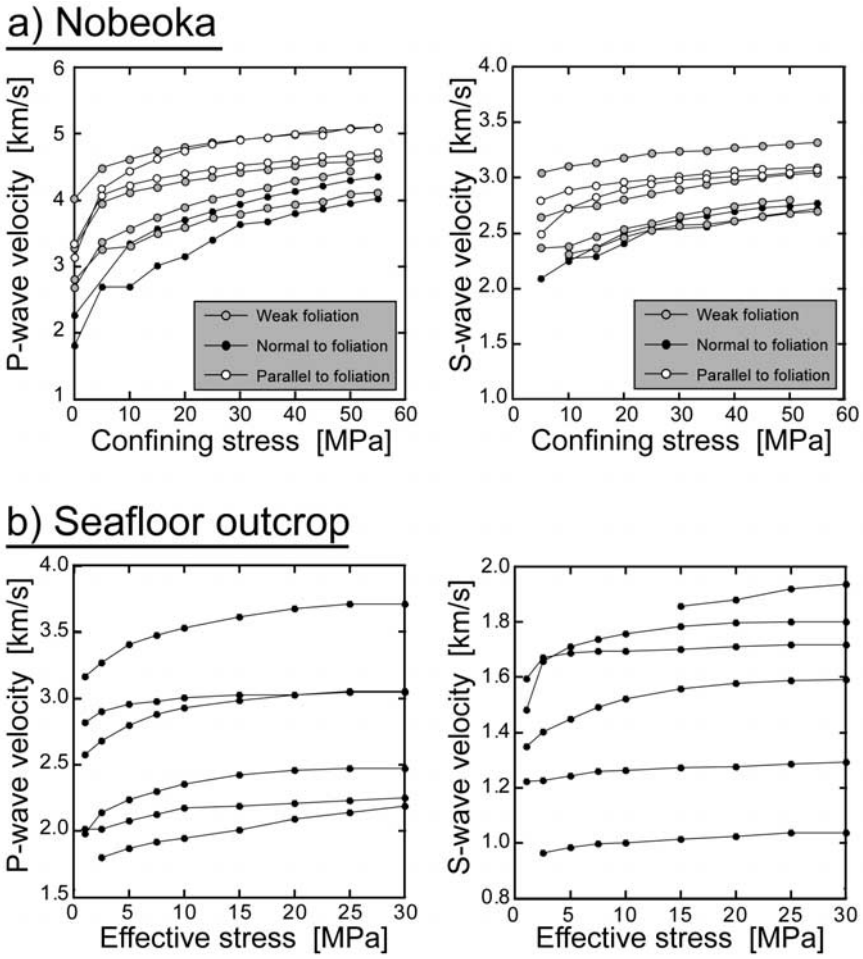

Figure 3. (a) Relationships between elastic velocities and pressure for the Nobeoka outcrop samples. (b) Examples of the relationship between elastic velocities and pressure for seafloor outcrop samples from the Nankai accretionary prism. For the seafloor outcrop samples, pore fluid pressure was generated in addition to the confining stress in order to obtain velocities from totally saturated samples.

transformers (LVDTs) were mounted on the core holder to measure axial displacement along two sides of each minicore.

4. Stress and Pressure Concepts in Plate Convergent Margin

4.1. Effective Stress

[20] Effective stress can be considered as stress that causes crack closure and affects seismic velocity [e.g., *Kuster and Toksoz*, 1974; *Toksoz et al.*, 1976] therefore effective stress can be estimated from seismic interval velocity. The effective stress estimated from seismic interval velocity should represent mean effective stress (effective pressure) σ'_m.

$$\sigma'_m = \left(\sigma'_1 + \sigma'_2 + \sigma'_3\right)/3 \tag{1}$$

where σ'_1 is maximum principal effective stress, σ'_2 is intermediate principal effective stress, and σ'_3 is minimum principal effective stress. Because we cannot estimate stress anisotropy from isotropic seismic velocities, we use the estimated mean effective stress for pressure prediction in this study. If we quantitatively consider stress state (principal stress direction) from seismic data, we should use velocity anisotropy and introduce anisotropic media (crack orientation) [e.g., *Hudson*, 1981; *Crampin*, 1985; *Jakobsen et al.*, 2000; *Peacock*, 2003; *Hayward et al.*, 2003].

[21] When we assume that the minimum and intermediate principal stresses are equal ($\sigma'_2 = \sigma'_3$) [*Moore and Tobin*, 1997], we can estimate the maximum and minimum principal stresses from mean effective stress using $R = \sigma'_3/\sigma'_1$ [*Moore and Tobin*, 1997]:

$$\sigma'_1 = (3/1 + 2R)\sigma'_m \tag{2a}$$

$$\sigma'_3 = (3R/1 + 2R)\sigma'_m. \tag{2b}$$

In undeformed sedimentary basin, the vertical effective stress σ'_v should be larger than the horizontal stress σ'_h and is considered as maximum stress σ'_1 (equation (2a) with $R = \sigma'_h/\sigma'_v = K_0$). Sediment underthrust beneath the décollement is not thrust faulted and probably approximates the undeformed basin state of stress ($R = \sigma'_h/\sigma'_v = K_0$; Figure 4a) [*Moran et al.*, 1993; *Moore and Tobin*, 1997]. However within the accreted sequence (Figure 4a), the vertical effective stress σ'_v should be lower than the

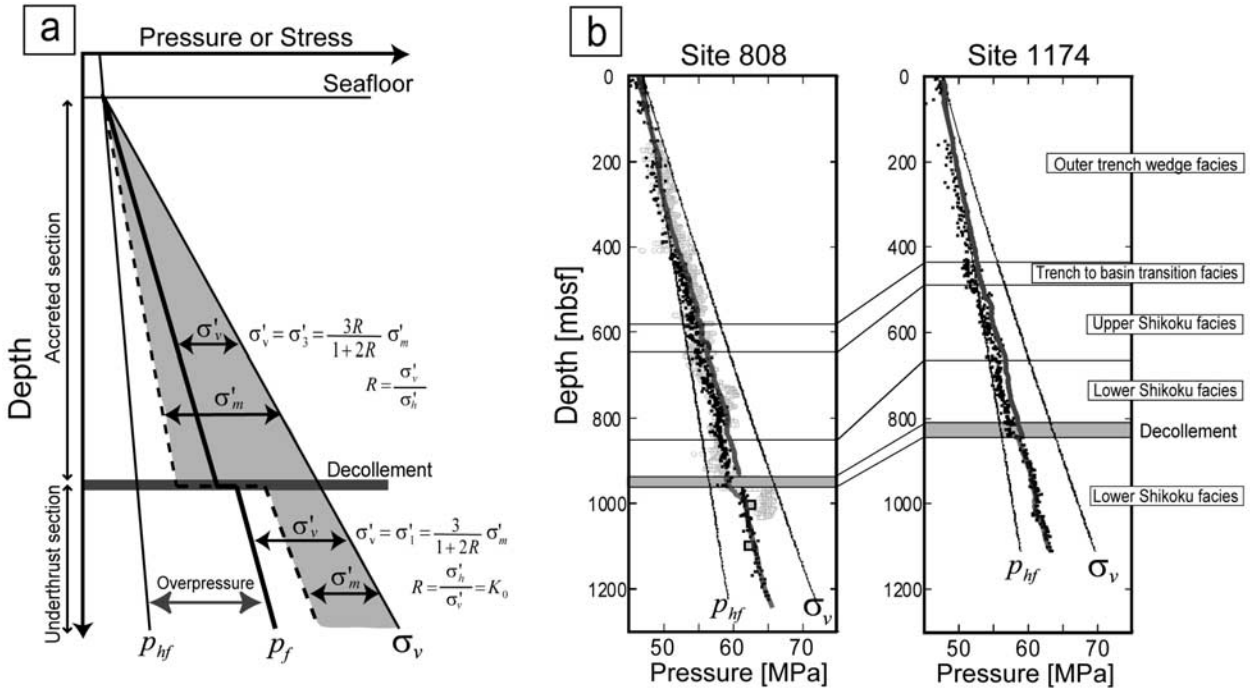

Figure 4. (a) Pressure concept in the accreted section and underthrust section. The width of gray zone represents the mean effective stress. We need to estimate vertical effective stress from mean effective stress, when we estimate pore pressure (equations (5) and (6)). (b) Pore pressure, hydrostatic pore pressure, and vertical confining stress at Sites 1174 and 808. Pore pressures predicted from porosities by using the *Rubey and Hubbert* [1959] relationship are shown as black dots [*Screaton et al.*, 2002; *Straub*, 2002; *Saffer*, 2003]. The pore pressures above the décollement is corrected by considering stress state (gray lines). Pore pressures predicted from logging-while-drilling densities are shown as open gray dots [*Ienaga*, 2003]. Pore pressures predicted by using a reconsolidation test [*Karig*, 1993] are shown as squares. mbsf = meters below seafloor.

horizontal stress σ'_h and can be considered as minimum effective stress σ'_3 (equation (2b) with $R = \sigma'_v/\sigma'_h$) [*Moran et al.*, 1993; *Moore and Tobin*, 1997; *Hayward et al.*, 2003; *McNeill et al.*, 2004]. Although the maximum principal stress direction may be changed seaward of the deformation front and the horizontal stress becomes the maximum principal stress within accretionary prism, we cannot determine the stress characteristics around the deformation front from seismic interval velocity. Therefore we assume that the sedimentary sequence above the décollement including the trench zone in our survey area has similar stress characteristics to the accreted sequence.

4.2. Confining Stress

[22] Confining stress (total stress or lithostatic stress) in the vertical direction (σ_v) is caused by the weight of overlying sediments, including the weight of pore fluids. Therefore vertical confining stress σ_v can be obtained by integrating the bulk density as follows:

$$\sigma_v(z) = g \int_0^z \rho(z')dz', \tag{3}$$

where ρ is the wet bulk density (including seawater above the seafloor), g is gravitational acceleration, and z is depth. On the other hand, the horizontal confining stress σ_h is much more difficult to estimate. As in the case of effective stress, the vertical confining stress obtained via equation (3) should be higher than horizontal confining stress in the underthrust sequence and lower than horizontal stress in the accreted sequence.

4.3. Pore Pressure

[23] When fluid–matrix interactions (pore elasticity) are ignored (Biot coefficient $\alpha = 1$) [e.g., *Biot*, 1955; *Christensen and Wang*, 1985], the pore fluid pressure p_f can be estimated using vertical confining stress obtained from density (equation (3)) and vertical effective stress:

$$p_f = \sigma_v - \sigma'_v. \tag{4}$$

[24] In the accreted sequence, the vertical effective stress is interpreted as minimum principal stress (Figure 4a) therefore equation (4) can be represented using the relation of equation (2b) [*Moore and Tobin*, 1997]:

$$\begin{aligned} p_f &= \sigma_v - \sigma'_3 \\ &= \sigma_v - (3R/1 + 2R)\sigma'_m. \end{aligned} \tag{5}$$

$R = \sigma'_3/\sigma'_1 = \sigma'_v/\sigma'_h$ within the Nankai accreted sequence was estimated 0.33–0.5 [*Moran et al.*, 1993]. Therefore when we obtain the mean effective stress from seismic interval velocities, pore fluid pressure can be estimated by subtracting the corrected vertical effective stress from the vertical confining stress (equation (5)).

[25] In the underthrust sequence, the vertical effective stress is interpreted as maximum principal stress (Figure 4a) therefore pore pressure can be estimated using equation (2a):

$$p_f = \sigma_v - \sigma'_1 = \sigma_v - (3/1 + 2R)\sigma'_m. \quad (6)$$

$R = \sigma'_3/\sigma'_1 = \sigma'_h/\sigma'_v = K_0$ in the sedimentary basin (normal vertically loaded sediment) is typically 0.4–0.5. However it is difficult to obtain R in the underthrust sequence, because R (or K_0) in the underthrust sequence is increasing from the deformation front to landward region. The large $R(\sigma'_h/\sigma'_v)$ in the underthrust sequence may allow the décollement step-down to the top of the oceanic crust, therefore $R(\sigma'_h/\sigma'_v)$ in the underthrust section of our study area should be less than 1.

4.4. Hydrostatic Pore Pressure and Over Pressure

[26] The hydrostatic pore pressure P_{hf} is a function of the height of the fluid column z and the fluid density ρ_w:

$$p_{hf}(z) = \rho_w g z. \quad (7)$$

Hydrostatic pressure is the pressure exerted by the weight of a static column of seawater (Figure 4a). Furthermore, when pore pressure is greater than hydrostatic pressure, the amount of overpressure (or excess pressure) is obtained by subtracting the hydrostatic pore pressure from the estimated pore pressure (Figure 4a). To evaluate the degree of overpressure in comparison to the hydrostatic effective stress (the difference between confining stress and hydrostatic pore pressure) in deep water environment, we used the normalized pore pressure ratio λ^* [e.g., *Shi and Wang*, 1988; *Screaton et al.*, 2002], defined as

$$\lambda^* = \frac{P_f - P_{hf}}{\sigma_m - P_{hf}}. \quad (8)$$

5. Pressure at Boreholes (Site 1174 and 808)

[27] Before estimating the pressure distribution within the accretionary prism, we needed to establish the effective stress and pore pressure profiles at the boreholes. From the bulk densities of core samples at Site 1173, the vertical effective stress in the lower Shikoku facies can be calculated from equations (3), (4), and (7), because Site 1173 can be assumed to be in a hydrostatic state (equilibrium state) [*Screaton et al.*, 2002; *Straub*, 2002; *Saffer*, 2003]; the hydrostatic pore pressure can be calculated from equation (7), and the vertical confining stress can be calculated from equation (3).

[28] From the estimated vertical effective stress and porosity of the lower Shikoku facies at Site 1173, the following relationship (as defined by *Athy* [1930]; *Rubey and Hubbert* [1959]) could be constructed:

$$\phi = \phi_0 e^{-\beta\sigma'_v}, \quad (9)$$

where ϕ_0 is a reference porosity, and β is related to the compressibilities of the sediments and pore water. For ϕ_0 of 0.66 and β of 0.115 in equation (9), the relationship fits that of the hydrostatic state of Site 1173 (lower Shikoku facies) [*Straub*, 2002].

[29] By using the constructed Rubey and Hubbert relationship (equation (9)), vertical effective stresses in sedimentary basin could be estimated from their porosity. However, because the accreted sediments above the décollement have been subjected to strong lateral compression in addition to vertical overburden, an analysis based on reference-site porosities (equation (9)) would overestimate vertical effective stress (dots in Figure 4b). Therefore the pore pressure estimated by subtracting the overestimating vertical effective stress from the vertical confining stress may be lower than the in situ value within the accreted sediments of Sites 1174 and 808 [*Moran et al.*, 1993; *Saffer*, 2007]. Here we assumed that the effective stress obtained from porosity represent mean effective stress within accreted sedimentary sequence. Then we could estimate vertical (minimum) effective stress using the equation (2b). We assumed $R = \sigma'_3/\sigma'_1$ within the accreted sequence as 0.45 [*Moran et al.*, 1993] and calculated the pore pressure in the accreted sequence (gray line in Figure 4b).

[30] On the other hand, the vertical effective stresses of the underthrust sequence at Sites 1174 and 808 could be estimated from their porosity by using the *Rubey and Hubbert* [1959] relationship constructed at Site 1173 (equation (9)) [*Screaton et al.*, 2002; *Straub*, 2002; *Saffer*, 2003], because their principal stress direction should be similar to the lower Shikoku facies of Site 1173. Then we easily obtained pore pressures in the underthrust sequence (dots in Figure 4b) by subtracting the estimated vertical effective stress from the vertical confining stress (equation (4)). Whereas the mean effective stress in the underthrust sequence should be calculated from the vertical (maximum) effective stress using equation (2a), because seismic velocity is affected by the mean effective stress. The mean effective stress at the boreholes (Site 1174 and 808) are depended on $R = \sigma'_3/\sigma'_1 = K_0$. However, as described later, although we correct vertical effective stress to mean effective stress at the boreholes and use them for pressure prediction in the underthrust sequence, the estimated mean effective stress needs to be converted again to the vertical effective stress, and the final result (vertical effective stress or pore pressure) becomes similar. Therefore we treated the vertical effective stress as mean effective stress in the underthrust sequence for the calculation of seismic velocity.

[31] The results of indirect pore pressure estimation derived from reconsolidation tests (squares in Figure 4b) [*Karig*, 1993] are consistent with the predicted pore pressure from the Rubey and Hubbert relationship (dots in Figure 4b) [*Screaton et al.*, 2002; *Straub*, 2002; *Saffer*, 2003]. The pore pressures were also predicted from logging-while-drilling (LWD) densities (open gray dots in Figure 4b) [*Ienaga*, 2003]. Below the décollement at Site 808 (gray zones in Figure 4b), the pore pressures estimated from LWD densities are higher than those from the Rubey and Hubbert relationship, mainly because of the fracturing near the décollement.

[32] The Rubey and Hubbert relationship is based on the concept that increasing effective stress causes pore space to collapse as rocks compact. Because decreasing effective

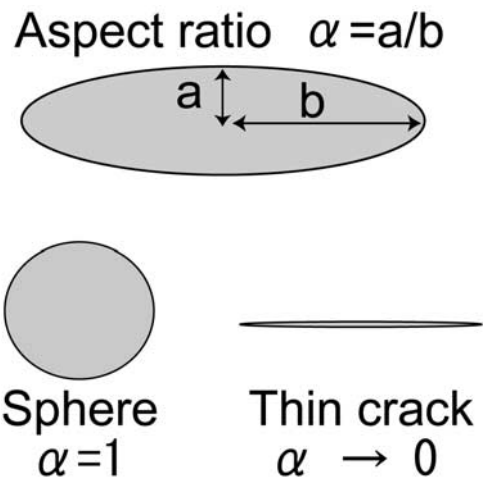

Figure 5. Description of ellipsoidal pores by aspect ratio.

stress due to fluid intervention or tectonic unloading creates thin cracks instead of rounded pores, it has little influence on total porosity. Therefore the Rubey and Hubbert relationship is inappropriate for the unloading lithology because the relationship during loading and unloading could be different. However, because high-pressure fluid intervention and tectonic unloading may not be dominant effects at drilling sites near the trough axis, we believe that pore pressures estimated via the Rubey and Hubbert relationship are reliable at Sites 1174 and 808 (Figure 4b). Furthermore, this method (equation (9)) ignores the lithological difference between trench-wedge facies, upper Shikoku facies, and lower Shikoku facies. Therefore the estimated pore pressures in the trench-wedge facies and upper Shikoku facies may contain errors. Cementation in the upper Shikoku facies at Site 1173 [e.g., *Spinelli et al.*, 2007] makes it difficult to obtain the Rubey and Hubbert relationship within the upper Shikoku facies. However, the lithological boundary marked by cementation at Site 808 is ambiguous compared to that of the undeformed Site 1173, party because of the deformation at Site 808. The predicted pore pressure in the lower Shikoku facies continues downward from the upper Shikoku facies (Figure 4b). Therefore we assumed that the Rubey and Hubbert relationship constructed in the lower Shikoku facies of Site 1173 (equation (9)) could be applied also to the trench-wedge facies and upper Shikoku facies at Sites 808 and 1174.

6. Rock Physics Model

6.1. Crack Closure With Increasing Mean Effective Stress

[33] The increase in *P* wave and *S* wave velocities as a function of increasing mean effective stress is caused by closing of thin cracks (Figures 5 and 6). To calculate the changes in elastic moduli as a function of mean effective stress, we estimated the rate of thinning and closing of the cracks as effective stress increased. In this study, the pore space is considered to be in the form of ellipsoidal pores, which can be described by an aspect ratio (Figure 5), and the rock is assumed to contain pores of various aspect ratios. Granular pores, which are dominant in sandstone, are modeled as rounded pores with large aspect ratios, whereas grain-to-grain contacts and micro-cracks in minerals are modeled as cracks with small aspect ratios [e.g., *Zhang and Bentley*, 2003].

[34] *Toksoz et al.* [1976] proposed an expression for the fractional change in the concentration of aspect ratio of an ellipsoidal pore (or the pore volumes with a particular aspect ratio) $dc(\alpha)$ for an mean effective stress σ'_m:

$$\frac{dc(\alpha)}{c(\alpha)} = \frac{-\sigma'_m}{K^*_A} \Big/ [F_1 - F_2F_3/(F_3 + F_4)], \tag{10}$$

where α and $c(\alpha)$ are the aspect ratio and its corresponding concentration (pore volume), respectively. The values of F_i are functions of aspect ratio α and some effective matrix moduli defined as the effective static matrix moduli of the rock with all the pores except those with aspect ratio α [*Toksoz et al.*, 1976]. K^*_A is the static bulk modulus of the dry rock, but because of the lack of such a static modulus it is taken to be the dynamic bulk modulus of the dry rock [*Cheng and Toksoz*, 1979]. When $dc(\alpha)/c(\alpha)$ is less than -1, as mean effective stress increases, the ellipsoidal cracks of aspect ratio α are completely closed, and the concentration of that aspect ratio $c(\alpha)$ is removed from the aspect ratio spectrum for the subsequent higher mean effective stresses.

6.2. Differential Effective Medium Theory

[35] To calculate the theoretical velocity from the aspect ratio spectrum of pore space, we used differential effective medium (DEM) theory [e.g., *Berryman*, 1980; *Norris*, 1985; *Berryman*, 1992]. DEM theory models two-phase composites by incrementally adding inclusions of one phase to a background matrix phase, and then recomputing the new effective background material at each increment [e.g., *Cleary et al.*, 1980; *Norris*, 1985; *Berge et al.*, 1992; *Mavko et al.*, 1998]. Therefore DEM theory can be applied to a relatively high-porosity medium [e.g., *Norris*, 1985; *Berge et al.*, 1992; *Xu and White*, 1995].

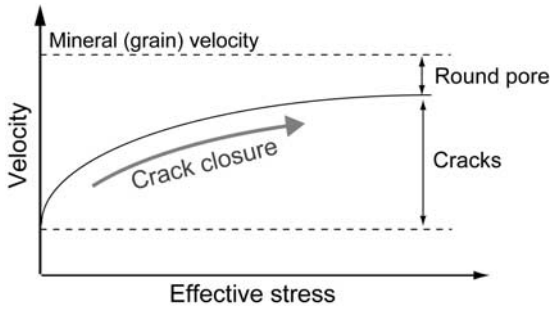

Figure 6. Parameters that constrain the relationship between effective stress and elastic velocity. The amount of velocity change with effective stress indicates the amount of crack-like pore space [*Mavko et al.*, 1998]. Rounded pores are not closed by increases of effective stress.

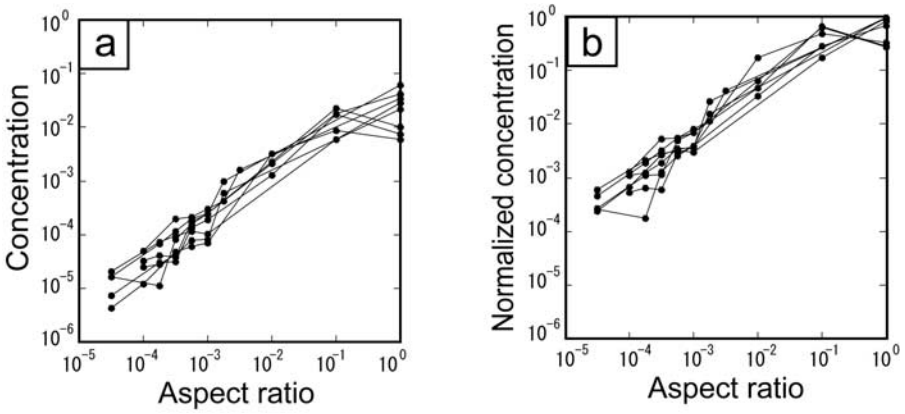

Figure 7. (a) Aspect ratio spectra and (b) normalized aspect ratio spectra of samples obtained from the footwall of the Nobeoka thrust. These spectra were obtained by inversion of velocity–pressure relationships. The footwall samples do not exhibit strong velocity anisotropy [*Tsuji et al.*, 2006].

[36] The coupled system of ordinary differential equations for the effective bulk and shear moduli, (K^* and μ^*) are

$$(1-y)\frac{dK^*(y)}{dy} = \left(K' - K^*\right)\frac{1}{3}T_{iijj}(y) \tag{11a}$$

$$(1-y)\frac{d\mu^*(y)}{dy} = \left(\mu' - \mu^*\right)\frac{1}{5}\left(T_{ijij}(y) - \frac{1}{3}T_{iijj}(y)\right) \tag{11b}$$

with initial conditions $K^*(0) = K_0$ and $\mu^*(0) = \mu_0$, where K_0 and μ_0 are elastic moduli of the initial host material (or grain elastic moduli) [*Norris*, 1985; *Berryman*, 1992; *Mavko et al.*, 1998]. K' and μ' are elastic moduli of the incrementally added inclusions. In this study, we assumed that the inclusions were seawater filled pores (K' = 2.25 GPa, μ' = 0 GPa). T_{iijj} and T_{ijij} are scalar quantities (geometrical coefficients) that are a function of aspect ratio, and of pore and grain elastic properties [*Kuster and Toksoz*, 1974]. y is the total concentration of inclusions added to the host material. When all inclusions have been added to the host material, y (equation (11)) equals total porosity

$$\phi_0 = \sum_{m=1}^{M} c(\alpha_m), \tag{12}$$

where $c(\alpha_m)$ is the concentration of the mth aspect ratio. M is the total number of the aspect ratio of open cracks in aspect ratio spectrum.

[37] This approach can describe overlapping pores [*Norris*, 1985]. First, large aspect ratio pores are added to the effective background material, followed by smaller aspect ratio cracks which have a greater effect on velocities [e.g., *Kuster and Toksoz*, 1974]. By applying the aspect ratio spectrum of the open cracks at each mean effective stress in DEM theory, we calculated the theoretical velocity parameterized by mean effective stress (Figure 6). To obtain low-frequency acoustic properties (relaxed fluid) by using DEM theory, we calculate elastic moduli of the dry frame (by adding dry inclusions to the host material), and then calculate the wet moduli by Gassmann fluid substitution [e.g., *Xu and White*, 1995; *Mavko et al.*, 1998].

[38] Since DEM theory neglects crack-to-crack interactions, it is difficult to apply the theory to a high-porosity medium such as that just below the seafloor. In such uncemented lithologies, we can use self-consistent (SC) theory [*O'Connell and Budiansky*, 1974], because SC theory treats grains and pores symmetrically without requiring a single background material and allows the composite medium to become disconnected at a finite porosity [*Berge et al.*, 1995; *Mavko et al.*, 1998]. However, because our primary target near the décollement is deep and of low porosity (<30%), it is a consolidated sequence that is appropriate for the DEM model.

7. Method and Results

[39] From the crack aspect ratio spectrum estimated from laboratory-derived properties and borehole data, we calculated a theoretical relationship between acoustic velocity and mean effective stresses by using DEM theory [*Norris*, 1985; *Berryman*, 1992]. We then iteratively fitted the theoretically calculated velocities to seismic interval velocities to estimate the mean effective stresses corresponding to those interval velocities. We then obtained pore pressure by subtracting the corrected vertical effective stress from the vertical confining stress.

7.1. Aspect Ratio Spectrum

[40] From the relationship between velocities and mean effective stresses determined from the samples obtained from the footwall of the Nobeoka thrust (Figure 3a) [*Tsuji et al.*, 2006], we estimated aspect ratio spectra $c(\alpha_m)$ by using Kuster–Toksoz theory (Figure 7a) [*Kuster and Toksoz*, 1974; *Cheng and Toksoz*, 1979]. Although we used DEM theory (equation 11) to predict pore pressures, we used Kuster–Toksoz theory to estimate the aspect ratio spectrum because it employs a simple inversion technique [*Cheng and Toksoz*, 1979] and the velocity differences derived by these two approaches (Kuster–Toksoz theory and DEM theory) are small for low-porosity rocks [e.g., *Ursenbach*, 2001]. In addition, because we characterized only the shape of the aspect ratio spectrum of our samples, the detailed differences from the two approaches are not important. The porosity of the seafloor outcrop samples (Figure 3b) are

high (>17%) and exceed the constraints imposed by *Kuster and Toksoz* [1974] on their theory. Therefore we did not estimate the aspect ratio spectrum of the seafloor outcrop sample by using Kuster and Toksoz theory and inversion.

[41] The estimated aspect ratio spectra $c(\alpha_m)$ (Figure 7a) were then normalized by dividing them by total porosity ϕ_0 (equation (12)) to obtain the normalized aspect ratio spectra (Figure 7b) [*Cerney and Carlson*, 1999; *Tsuji and Iturrino*, 2008]:

$$c_{nor}(\alpha_m) = c(\alpha_m) \Big/ \sum_{m=1}^{M} c(\alpha_m). \tag{13}$$

Because the normalized concentrations $c_{nor}(\alpha_m)$ increase linearly with normalized aspect ratio α_m on logarithmic coordinates (Figure 7b), we assumed that

$$\mathrm{c}_0(\alpha_i) = \alpha_{\mathrm{i}}^{E} \qquad \left(10^{-4.8} \le \alpha_i \le 1\right). \tag{14}$$

E in equation (14) is a quantity that determines pore features. Lithologies with large E values are dominated by rounded pores (those with large aspect ratios). Therefore a lithology with a large E value indicates sand dominance. On the other hand, mudstone is dominated by thin cracks and has a small E value. By multiplying the normalized aspect ratio spectrum representing open pores by in situ porosity, we can determine the aspect ratio spectrum $c(\alpha_m)$ at in situ effective stress.

[42] The range of aspect ratios in equation (14) also affects the pressure dependence of velocities. Therefore we calculated the theoretical velocity by applying DEM theory to the modeled aspect ratio spectrum (equation (14)) and determined the range of aspect ratios by comparing the theoretically calculated P wave and S wave velocities with the velocities determined experimentally from rock samples (Figure 3). In this study, the range of aspect ratios we used was $10^{-4.8}$–1, and we configured a total of 69 different aspect ratios in order to model the aspect ratio spectrum. The velocity–stress relationships parameterized by E (Figure 8a) reveal that E clearly characterizes velocity–stress relationships therefore the assumption of the linear relationship on logarithm coordinates between aspect ratio and its concentration (equation (14)) is plausible. Furthermore, when we assume a constant E value, we can obtain velocity–stress relationships parameterized by porosity (Figure 8b).

7.2. Aspect Ratio Spectra at Boreholes

[43] From grain elastic moduli of the mixture of minerals, porosity, density, and mean effective stress at the boreholes, we calculated theoretical velocities parameterized by E (aspect ratio spectrum) by using DEM theory (Figure 8a). We then determined E by iteratively fitting the theoretically calculated acoustic velocities to the seismic interval velocities recorded at the boreholes. Cracks gradually become thinner (aspect ratios decrease) with increasing depth, and thin cracks are eventually closed. When increased mean effective stress has closed the cracks (equation (10)), the theoretical velocity calculated using DEM theory increases (Figure 6). When pore pressure at the borehole is predicted using the estimated value of E, the predicted pore pressures are consistent with the pressure calculated from the Rubey and Hubbert relationship (Figure 9). Therefore we have confirmed that E was accurately determined at the boreholes.

[44] Ideally, a precise determination of E requires laboratory experiments (velocity–stress relationships) on borehole samples so that E at the sampling points can be calculated by fitting the theoretical velocity–stress relationships to the measured relationships of the samples. However, we do not have laboratory-derived velocities of borehole samples under effective stress.

7.3. Effective Stress and Pore Pressure Distribution

[45] If E values within the accretionary prism are determined by interpolating and extrapolating E values estimated at Sites 1173, 1174, and 808, we can calculate the theoretical velocity parameterized by mean effective stress by using DEM theory from grain elastic moduli, density, and aspect ratio spectra obtained by multiplying the normalized aspect ratio spectrum by open porosity at that mean effective stress. However, it is difficult to predict the pore pressure distribution landward of the deformation front by interpolating and extrapolating E values at the boreholes, because there are only three boreholes, and they are near the deformation front. Therefore E should be constrained by any of the properties that can be derived from seismic attributes. In this study, E was constrained by porosity. The dominant aspect ratio (E in this study) may depend on clay content [e.g., *Xu and White*, 1995], and the clay content (measured with natural gamma ray well logs) has a linear relationship with porosity at Sites 1173 and 808. This linear relationship is in part attributable to sediment compaction due to increased mean effective stress with depth [*Mikada et al.*, 2002]. However, *Steurer and Underwood* [2003] reported on laboratory experiments that showed that porosity has a linear relationship with clay content [e.g., *Shipboard Scientific Party*, 2001a, 2001b]. These observations demonstrate that porosity can be assumed to be the quantity that characterizes the aspect ratio spectrum (E) in our study area. Therefore, by constructing the relationship between porosity and E, we can obtain the aspect ratio spectrum (E distribution) within the accretionary prism from porosity.

[46] Because both porosity and E were estimated at the boreholes, we can construct the relationship between E and porosity (Figure 10a). Furthermore, because we could not obtain this relationship in the low-porosity range from only borehole data near the deformation front, we estimated E values by fitting the theoretically calculated velocities–stress relationships to the effective stress dependence of velocities determined from the Nobeoka outcrop samples (Figure 3a) [*Tsuji et al.*, 2006]. When E is ~0.9 for the low-porosity Nobeoka samples (squares in Figure 10), the theoretically calculated velocities are consistent with the velocities of the Nobeoka outcrop samples (Figure 11a). From the velocities of seafloor outcrop samples (Figure 11b), furthermore, we estimated E for a higher porosity range (solid dots in Figure 10). For seafloor outcrop samples of high porosity, however, it is difficult to fit the theoretical velocities to laboratory-derived velocities because the theory neglects crack-to-crack interactions. Two seafloor outcrop samples have high E *value*s (black arrows in Figure 10) because they are sandstone samples with pores of large aspect ratio [*Xu and White*, 1995].

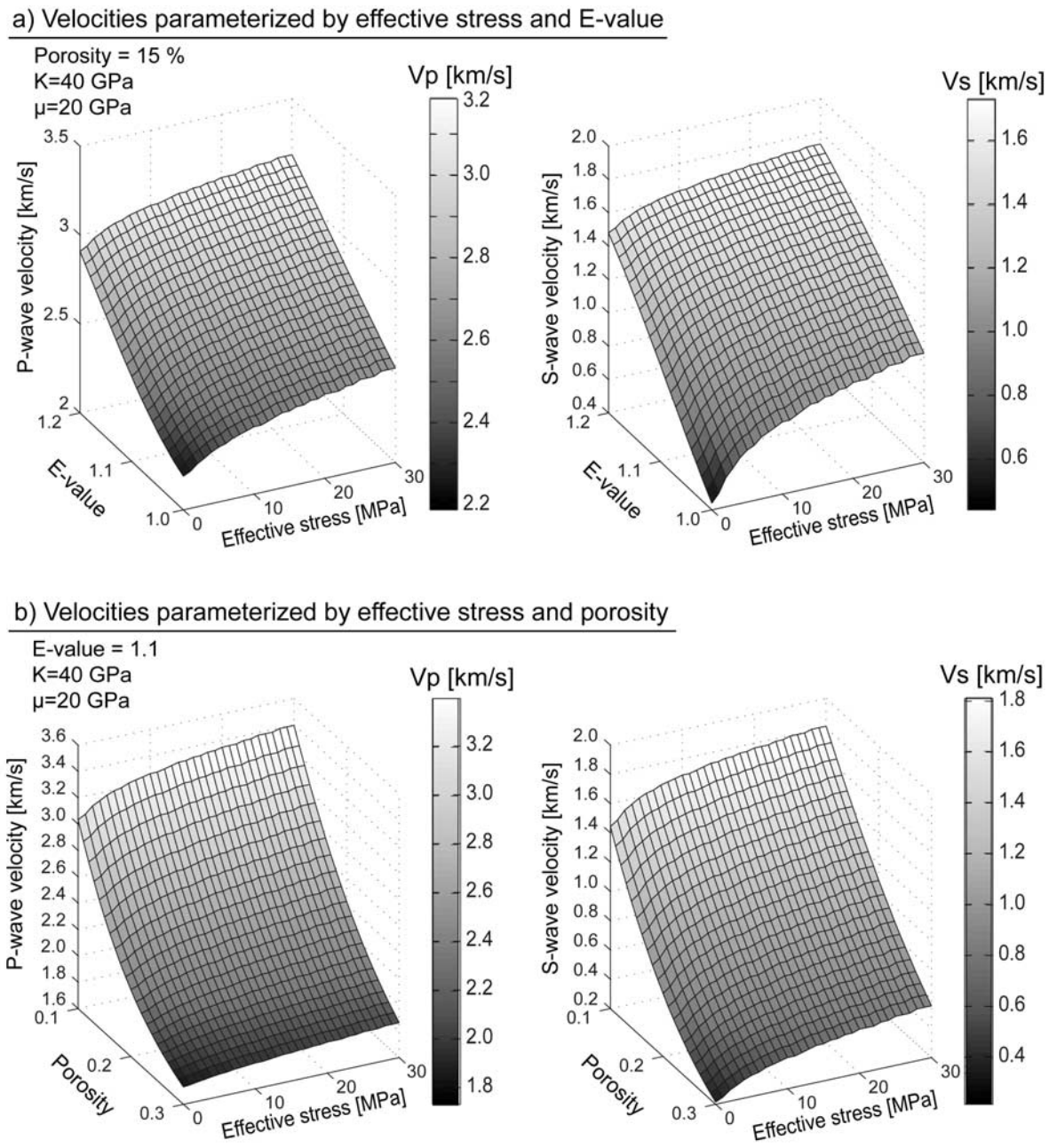

Figure 8. (a) Velocities parameterized by effective stress and E. These relationships were obtained for porosity of 15%. (b) Velocities parameterized by effective stress and porosity. These relationships were obtained for $E = 1.1$.

[47] The clear relationship between E and porosity (Figure 10a) demonstrates that E is well represented by porosity. From the relationship between E and porosity (Figure 10a), furthermore, we can obtain the proportion of crack porosity to total porosity (Figure 10b). From Figure 10b, we can see that low-porosity samples have a large proportion of thin crack porosity.

7.3.1. Pressure Prediction Using a Single Relationship Between E and Porosity

[48] Using a single relationship between E and porosity (thick gray line in Figure 10), we constructed the aspect ratio spectrum (E) within the accretionary prism from the porosity distribution. In this study, porosity within the accretionary prism was estimated by using an empirical relationship [e.g., *Hoffman and Tobin*, 2004], because it is difficult to estimate porosities by interpolating and extrapolating the properties from only a few boreholes. Because seismic interval velocities are little different from the acoustic velocities of borehole samples and sonic logs [*Costa Pisani et al.*, 2005], we constructed the relationship between seismic interval velocity and porosity at the boreholes by using the *Hoffman and Tobin* [2004] relationship to allow us to estimate the porosity distribution within the accretionary prism.

[49] We calculated the theoretical velocity from mean effective stress by applying DEM theory to the grain elastic

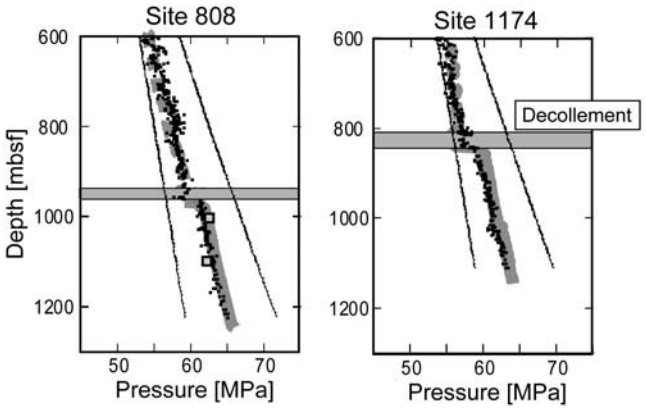

Figure 9. Predicted pore pressure profiles near the décollement (gray horizontal band) at Sites 808 and 1174. Pressures predicted from porosities by using the *Rubey and Hubbert* [1959] relationship (Figure 4b) are shown as small black dots [*Screaton et al.*, 2002; *Straub*, 2002; *Saffer*, 2003]. Pressures determined by reconsolidation test [*Karig*, 1993] are shown as gray squares outlined in black. The hydrostatic pore pressure and vertical confining stress are represented as straight lines. Above the décollement, pore pressure is not estimated using the corrected vertical effective stress via equation (5). Here we just compare the estimated pressure with the pore pressure obtained via Rubey and Hubbert relation (Figure 4b) for error estimation. The décollement is represented by a horizontal gray band.

moduli, density, and aspect ratio spectrum obtained from both E and open porosity at that mean effective stress. We assumed the initial mean effective stress to be hydrostatic. Under hydrostatic conditions, the theoretical velocity is much higher than the seismic interval velocity, because in situ mean effective stress is lower than that under hydrostatic conditions. By iteratively changing mean effective stress, we achieved a better match between the theoretical velocity and interval velocity, which allowed us to predict the mean effective stress (Figure 12a).

[50] Because we treated vertical effective stress as mean effective stress in the underthrust section at the boreholes, the estimated effective stress should be vertical stress. Therefore we need to estimate mean effective stress from the vertical stress in the underthrust section using equation (2a). However it is difficult to determine $R = \sigma_3'/\sigma_1' = K_0$, because R should increase from the deformation front to landward region in the underthrust sequence; R near the deformation front should be ~0.5, and R at the landward of our study area should be ~1. Because we cannot estimate R for the whole underthrust sequence in our study area, we use R = 0.75 for mean effective stress prediction in the underthrust section (Figure 12a).

[51] For the pore pressure prediction within the accreted section, the vertical effective stress needs to be calculated from the estimated mean effective stress (equation (5)). We then predicted pore fluid pressure by subtracting the corrected vertical effective stress from the vertical confining stress (Figures 12b and 12c). We show the excess pore pressure distribution in Figure 12b, because hydrostatic pressure increases by ~10 MPa/km and it is difficult to reveal overpressure on total pore pressure profile.

[52] The estimated pore pressure and the pressure assuming compaction disequilibrium at the boreholes (Figure 12d) are consistent at Site 808. However, this is not the case at Site 1174; the estimated pore pressure just below the décollement is higher than the pore pressure determined

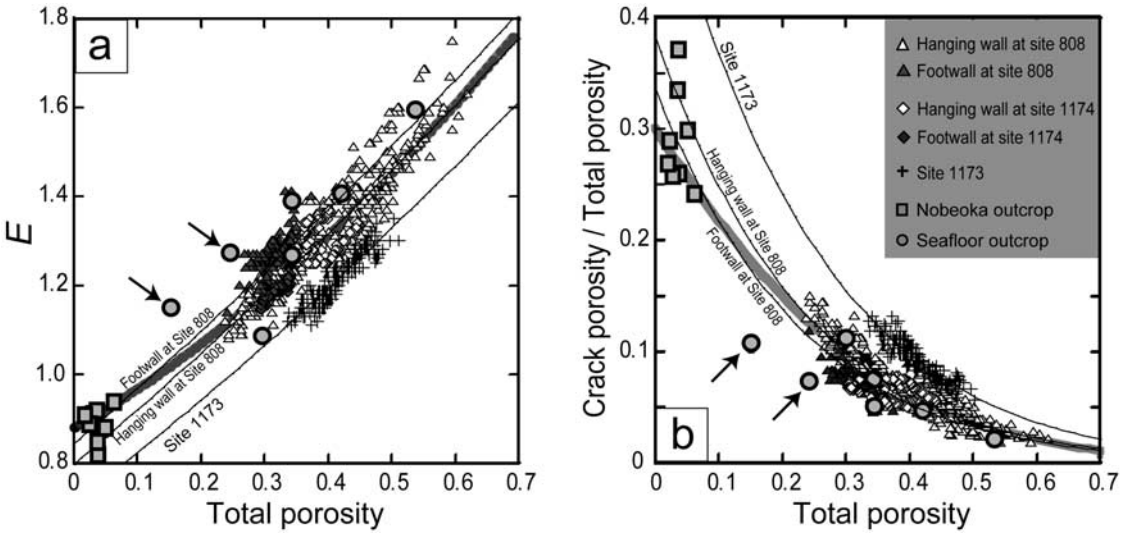

Figure 10. (a) Relationships between E and porosity. Triangles, rhombuses, and crosses represent the relationships obtained at Site 808, 1174, and 1173, respectively. Gray-filled squares and dots represent the relationships obtained from the Nobeoka outcrop samples and the seafloor outcrop samples, respectively. The thick gray line represents a single relationship between E and porosity incorporating data from the three boreholes, and the thin lines represent relationships at each borehole. The relationships at Site 1174 are not shown because they would make these figures too complex. The relationships of two seafloor outcrop samples (black arrows) show high values of E because these samples are dominantly sand. (b) Relationship between the proportion of crack porosity to total porosity. Crack porosity is defined here as the summed porosity of cracks of aspect ratio <0.05.

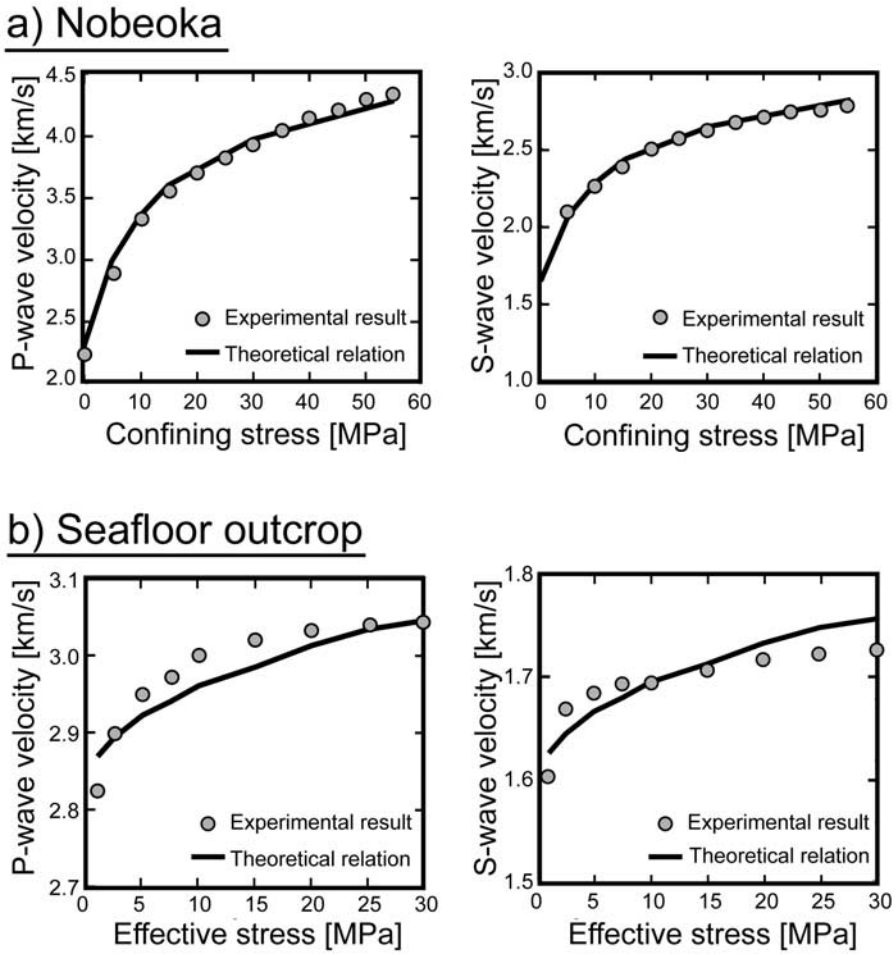

Figure 11. Comparison of theoretical and measured velocity–stress relationships for (a) Nobeoka outcrop samples and (b) seafloor outcrop samples.

from the Rubey and Hubbert relationship. This error reflects the assumption of a single relationship between E and porosity (thick gray line in Figure 10). The error originated from the relation between E value and porosity is approximately ±3 MPa.

[53] When E is estimated from porosity by using a single relationship (thick gray line in Figure 10) and constant grain elastic moduli are assumed, a theoretical relationship is obtained between velocity and porosity parameterized by mean effective stress (Figure 13). These relationships are similar to those shown in Figure 8b, although the former were obtained using a relationship between E and porosity (Figure 10). The theoretical relationships show that the P wave velocity of rock with 20% porosity increases by ~900 m/s as mean effective stress increases from 0 to 20 MPa. Furthermore, the relationship agrees well with the relationship between seismic interval velocity and porosity. This result demonstrates that mean effective stress can be obtained from the velocity–porosity relationship when elastic moduli are constant and a single relationship between E and porosity is assumed.

[54] The results we obtained by using a single relationship between E and porosity (Figures 12a–12d) are similar to those obtained by the Rubey and Hubbert relationship (equation (5)) [*Tobin and Saffer*, 2003], although we considered lithology (grain elastic moduli) differences and included laboratory-derived velocity–pressure relationships in our approach. We now consider cementation [e.g., *Morgan et al.*, 2007] and its effect on crack sealing.

7.3.2. Pressure Prediction Considering Crack Sealing

[55] From the relationship between E (crack aspect ratio) and porosity (Figure 10a), we can consider cementation associated with heating, which may increase seismic velocity. Figure 10a shows that for constant porosity, E increases slightly in the landward direction (from Site 1173 to Site 808). Because this landward increase of E represents increased dominance of rounded pores, this trend may reflect sealing of thin cracks because of heating, or changes to pore aspect ratios as a result of compaction. Because thin cracks soften grain-to-grain contacts, which in turn lowers seismic velocity, the closure of thin cracks to the landward region has a marked effect on the velocity–stress relationship (Figure6). To consider the effect of crack sealing, we interpolated and extrapolated the relationships between E and porosity at Sites 1173, 1174, and 808 (thin lines in Figure 10), and considered the effect of cementation in the direction of subduction. For the relationship between E and porosity, we observed that trends were different in the accreted sequence from those in the underthrust sequence; the relation in the underthrust section has larger change compared to that in the accreted

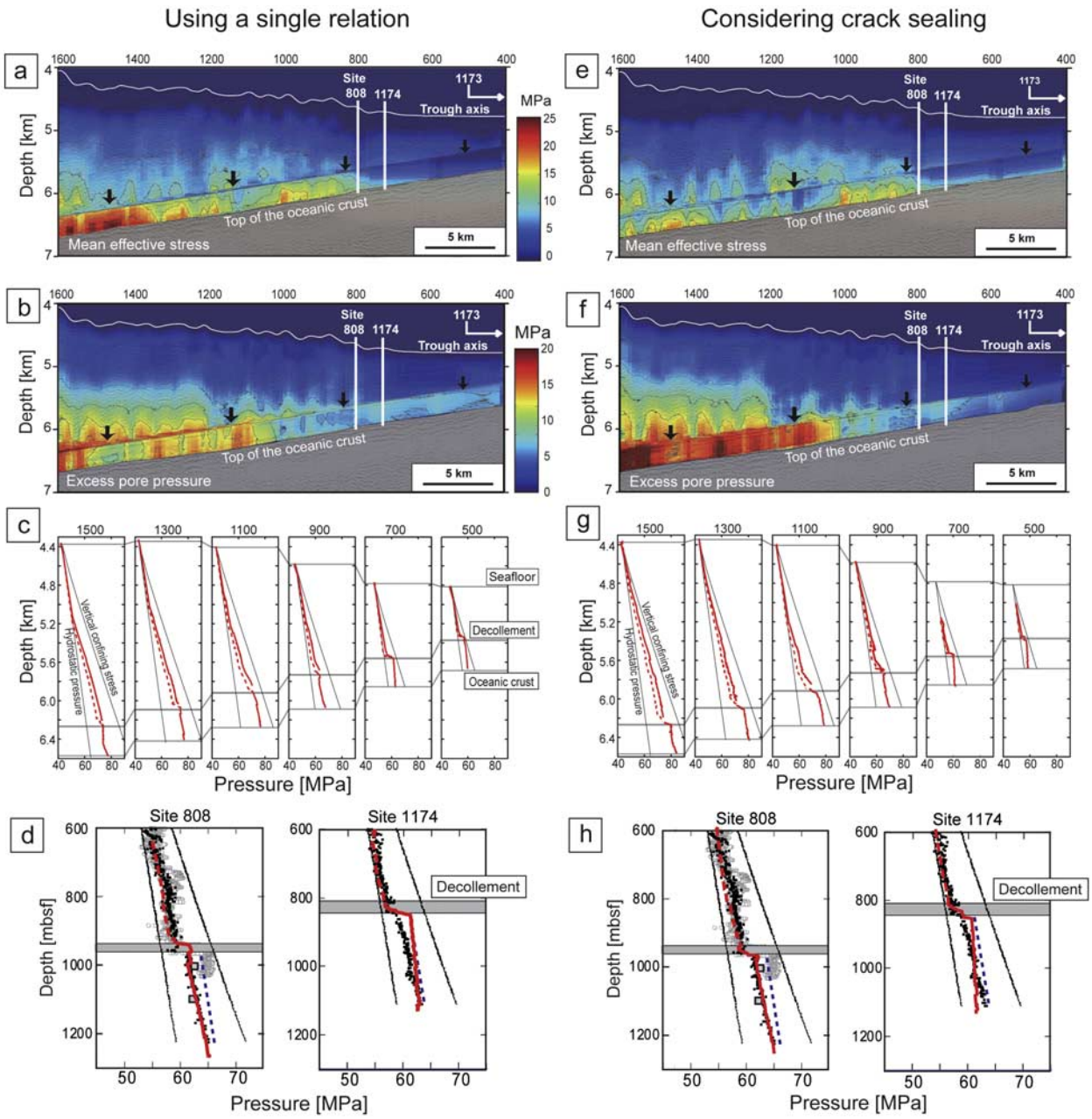

Figure 12. (a) Mean effective stress, (b) excess pore pressure, (c) pore pressure profile every 200 crosslines, and (d) pore pressure profile at the borehole estimated using a single relationship between E and porosity. Panels (e) to (h) present the same data as (a) to (d), but estimated using multiple relations between E and porosity. The numbers above the profile represent xline common mid point numbers. In (a), (b), (e), and (f), downward arrows show the décollement. In (a) and (e), mean effective stress in underthrust sequence were corrected using estimated vertical effective stress and $R = \sigma'_h/\sigma'_v = 0.75$ (equation (2b)). In (b) and (f), excess pore pressure above the décollement were corrected using $R = \sigma'_v/\sigma'_h = 0.45$ (equation (5)). In (c) and (g), the red lines above the décollement represent the corrected pore pressure, and the dashed red lines above the décollement represent uncorrected pore pressure. In (d) and (h), the predicted pore pressures are represented by red line. Pore pressures predicted from porosities by using the *Rubey and Hubbert* [1959] relationship (Figure 4b) are shown as black dots [*Screaton et al.*, 2002; *Straub*, 2002; *Saffer*, 2003]. In (d) and (h), we just compare the estimated pressure with the pore pressure obtained via Rubey and Hubbert relation (Figure 4b) for error estimation, therefore pressure above the décollement (dashed red lines) is not corrected considering prominent stress direction (equation (5)). Pressures from logging-while-drilling densities are represented as open gray dots [*Ienaga*, 2003]. Pressures from the reconsolidation test [*Karig*, 1993] are shown as squares. The dashed blue lines below the décollement indicate pore pressures expected for an undrained scenario, calculated assuming a uniform thickness of incoming sediment [*Saffer*, 2003].

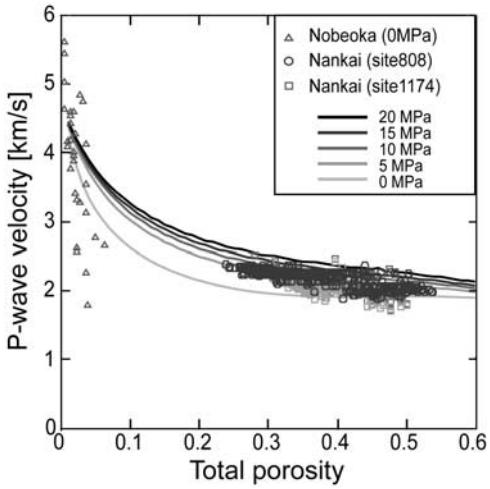

Figure 13. Theoretical relationship between velocity and porosity for mean effective stress from 0 to 20 MPa when a single relationship between E and porosity (thick gray line in Figure 10) and constant grain elastic moduli are assumed. The relationships between seismic velocity and porosity at Sites 1174 and 808, and Nobeoka outcrop are also shown.

section. Therefore we constructed different relationships for the accreted and underthrust sequences.

[56] From grain elastic moduli, density, and the estimated aspect ratio spectrum, we calculated the theoretical velocity parameterized by mean effective stress by using DEM theory. The theoretically calculated velocity was fitted to the seismic interval velocity by using mean effective stress as a fitting parameter. We then estimated the mean effective stress (Figure 12e) and pore pressure (excess pore pressure; Figure 12f). The predicted pore pressure within the underthrust sequence (Figures 12e–12g) is a little higher than that obtained using a single relationship between E and porosity (Figures 12a–12c), because we changed the relationship between E and porosity in the landward direction to account for cementation. Comparison of the predicted pore pressures with the pressures obtained from the Rubey and Hubbert empirical relationship at the borehole (Figure 12h) shows that the two methods provide consistent results at Site 808. Although the results obtained at Site 1174 are less consistent (Figure 12h), the average value of pore pressure of the underthrust sequence at Site 1174 is consistent.

7.4. S Wave Velocity and Poisson's Ratio

[57] If the aspect ratio spectrum (E) can be accurately calibrated with borehole data and laboratory-derived P wave and S wave velocities under mean effective stress, we can estimate S wave velocities within the accretionary prism by using DEM theory (Figure 14a). From the seismic interval (P wave) velocity (Figure 2b) and the estimated S wave velocity (Figure 14a), furthermore, Poisson's ratio can be estimated (Figure 14b). We found that Poisson's ratio ranges from 0.25 to 0.4 within the accretionary prism; this range is

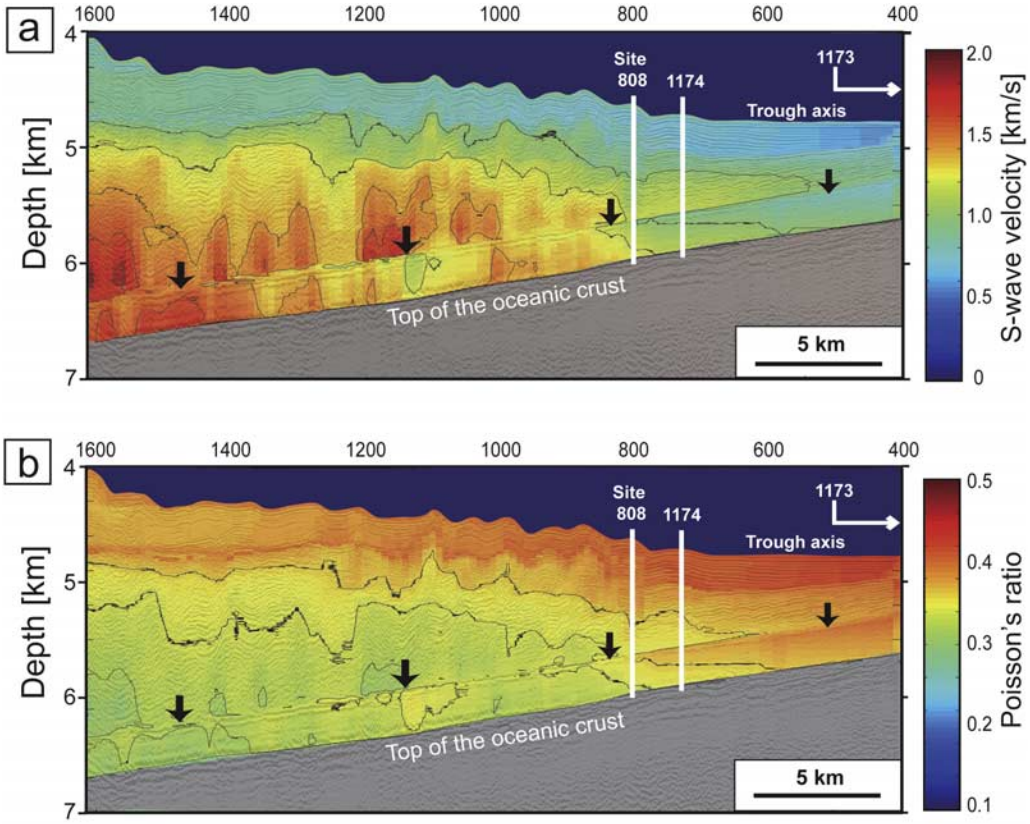

Figure 14. (a) S wave velocity within the accretionary prism estimated from aspect ratio spectrum by using DEM theory, (b) Poisson's ratio within the accretionary prism.

consistent with values determined in previous studies [e.g., *Takahashi et al.*, 2002].

8. Interpretation

[58] We obtained two mean effective stress and pore pressure models: (1) pressure predicted using a single relation between E and porosity (Figures 12a–12c) and (2) pressure predicted using multiple relations (Figures 12e–12g). Although pore pressure in the underthrust sequence is a little different between the results, the overall pore pressure trend is consistent. Our results confirm that abnormal high pore pressure occurs within the subducting sedimentary sequence (Figures 12c and 12g); the normalized pore pressure ratio (λ^* in equation (8)) is 0.4–0.7 within the underthrust sequence. The normalized pore pressure ratio λ^* of the underthrust sequence are consistent with a steady-state hydrologic model that accounts for sediment compaction and smectite dehydration [*Saffer and Bekins*, 1998] and pressure predicted assuming compaction disequilibrium [*Tobin and Saffer*, 2003]. This high pore fluid pressure within the underthrust sequence can account for aseismic slip due to the weak coupling along the décollement [e.g., *Hubbert and Rubey*, 1959; *Scholz*, 1998] and shallowly tapered geometry of the accretionary prism off the Muroto peninsula [e.g., *Davis et al.*, 1983].

[59] Seismic profiles (Figure 2) image the tectonic thickening of the accretionary prism that has occurred following displacement along the imbricate thrusts (e.g., frontal thrust), and the thickened prism increases the overburden load to the underthrust sequence. Furthermore the rapid turbidite sedimentation near the trough axis also increases overburden load. This increasing weight of the overburden decreases porosity. However, because pore fluid within the underthrust sequence may be sealed by a low bulk permeability marine sediment [*Gamage and Screaton*, 2006], the pore fluid has nowhere to escape and starts to carry some of the weight of the overburden. The increase in overburden load and low permeability sediment may increase the pore pressure of the underthrust sequence. Furthermore, the permeability near the décollement has strong anisotropy [e.g., *Tobin et al.*, 2001]; the permeability across the décollement (vertical direction) is low. The low permeability barrier across the décollement [*Brown et al.*, 1994; *Tobin et al.*, 2001; *Ujiie et al.*, 2003] may cause the pore pressure contrast at the décollement [e.g., *Tsuji et al.*, 2005a].

[60] The high pore pressure is not only due to compaction disequilibrium regime [*Swarbrick and Osborne*, 1998], but is also developed as a result of clay dehydration [e.g., *Powers*, 1959; *Burst*, 1969], fluid migration [e.g., *von Huene and Lee*, 1982], and breakdown of cementation [e.g., *Morgan et al.*, 2007]. Especially the Muroto transect is located above the extinct spreading ridge where the basement temperature is significantly high ~110°C [*Taira et al.*, 1991] therefore the high temperatures compared to other Nankai Trough regions have accelerated mineral diagenetic reactions [*Underwood et al.*, 2001; *Ujiie et al.*, 2003; *Morgan et al.*, 2007].

[61] The abnormal pore pressure within the underthrust sequence initiates seaward of the deformation front (Figure 12). The overpressure seaward of the deformation front may be caused by turbidite sedimentation or pore pressure transmitted from the landward underthrust sequence. If the seismic interval velocity (Figure 2b) was accurately determined, the pore pressure contrast at the décollement seaward of the deformation front suggests that the low-permeability seal across the décollement is developed from the seaward region of the deformation front [*Screaton et al.*, 2002; *Bangs and Gulick*, 2005; *Costa Pisani et al.*, 2005].

[62] The overpressure within the accreted sequence above the décollement initiates from the deformation front to the landward region (Figure 12). The increase in horizontal compaction within the accreted sequence [e.g., *Ienaga et al.*, 2006] may originate abnormal pore fluid pressure. Furthermore because the development of the imbricate thrusts (brittle failure) collapses the permeability barrier, high-pressure fluid migration from the underthrust sequence may partially generate abnormal pressure.

[63] The pore pressure contrast at the décollement is smaller to the landward region. In the landward of our study area, furthermore, the mean effective stress in the underthrust sequence is higher than that in the accreted sequence (Figures 12a and 12e). The higher effective stress in the underthrust sequence should be partially originated by increasing the ratio of horizontal stress to vertical stress from seaward to landward underthrust sequence, although we used constant $R = K_0 = 0.75$ for whole underthrust sequence in our study area. The decreasing pore pressure contrast across the décollement and changing R to landward may cause décollement step-down and development of out-of-sequence thrust.

9. Summary

[64] 1. To delineate mean effective stress and pore pressure within the Nankai accretionary prism off the Muroto peninsula, we developed a theoretical method using DEM theory and aspect ratio spectrum of pore space. When we estimated mean effective stress and pore pressure, we considered compressive state of stress in the accretionary prism.

[65] 2. The results demonstrate abnormally high pore pressure within the underthrust sequence ($\lambda^* = 0.4 \sim 0.7$). The increase in vertical load by the prism thickening and low permeability barrier at the décollement may increase the pore pressure of the underthrust sequence.

[66] 3. Abnormal pore pressure within the underthrust sequence initiates seaward of the deformation front, probably due to turbidite sedimentation or pore pressure transmission. The pore pressure contrast at the décollement seaward of the deformation front suggests that the low-permeability seal across the décollement is developed from the seaward region of the deformation front.

[67] 4. Overpressuring within the accreted sequence is initiated at the deformation front and proceeds landward, probably due to the increase in horizontal compaction.

[68] 5. The pore pressure contrasts at the décollement become smaller landward of the deformation front. They may cause décollement step-down and development of out-of-sequence thrust further landward (outside) of our study area.

[69] **Acknowledgments.** We are grateful N. Bangs, T. Shipley, S. Gulick (Univ. Texas), S. Kuramoto (JAMSTEC), and Y. Nakamura (Univ. Tokyo) for their help with the acquisition of seismic reflection data, and J. Ashi (Univ. Tokyo), M. Hato (ERSDAC), T. Matsuoka (Kyoto Univ.), O. Nishizawa (AIST), and H. Tobin (Univ. Wisconsin-Madison) for helpful comments. Comments and suggestions by two anonymous reviewers greatly improved this paper. J. Ashi (Univ. Tokyo), Y. Ogawa (Tsukuba Univ.) and K. Kawamura (FGI) provided the seafloor outcrop samples obtained by submersible "*Shinkai 6500*" (JAMSTEC), and S. Onozuka (JOGMEC) helped us the measurements of velocities. This research was supported by the programs of the Grant-in-Aid for JSPS Fellows (18.10775) and Grant-in-Aid for Young Scientists (B) from the Japan Society for the Promotion of Science (20760568).

References

Ando, M. (1975), Source mechanisms and tectonic significance of historical earthquake derived from tsunami data, *Phys. Earth Planet. Inter.*, *28*, 320–336.

Athy, L. F. (1930), Density, porosity and compaction of sedimentary rocks, *Am. Assoc. Pet. Geol. Bull.*, *14*, 7675–7708.

Avseth, P., T. Mukerji, and G. Mavko (2005), *Quantitative Seismic Interpretation*, Cambridge Univ. Press, U.K.

Bangs, N. L., and S. P. S. Gulick (2005), Physical properties along the developing décollement in the Nankai Trough: Inferences from 3-D seismic reflection data inversion and Leg 190 and 196 drilling data, in *Proc. ODP, Sci. Results*, 190/196 [Online], edited by H. Mikada et al., available at http://www-odp.tamu.edu/publications/190196SR/354/354.htm.

Bangs, N. L., T. H. Shipley, and G. F. Moore (1996), Elevated fluid pressure and fault zone dilation inferred from seismic models of the northern Barbados Ridge décollement, *J. Geophys. Res.*, *101*, 627–642.

Bangs, N. L., T. H. Shipley, J. C. Moore, and G. F. Moore (1999), Fluid accumulation and channeling along the northern Barbados Ridge décollement thrust, *J. Geophys. Res.*, *104*, 20,399–20,414.

Bangs, N. L., T. Shipley, S. Gulick, G. Moore, S. Kuramoto, and Y. Nakamura (2004), Evolution of the Nankai Trough décollement from the Trench into the seismogenic zone: Inferences from three-dimensional seismic reflection imaging, *Geology*, *32*, 273–276.

Berge, P. A., G. J. Fryer, and R. H. Wilkens (1992), Velocity–porosity relationships in the upper oceanic crust: Theoretical considerations, *J. Geophys. Res.*, *97*, 15,239–15,254.

Berge, P. A., B. P. Bonner, and J. G. Berryman (1995), Ultrasonic velocity–porosity relationships for sandstone analogs made from fused glass beads, *Geophysics*, *60*, 108–119.

Berryman, J. G. (1980), Long-wavelength propagation in composite elastic media—II. Ellipsoidal inclusions, *J. Acoust. Soc. Am.*, *68*, 1820–1831.

Berryman, J. G. (1992), Single-scattering approximations for coefficients in Biot's equations of poroelasticity, *J. Acoust. Soc. Am.*, *91*, 551–571.

Biot, M. A. (1955), Theory of elasticity and consolidation for a porous anisotropic solid, *J. Appl. Phys.*, *26*, 115–135.

Brown, K. M., B. Bekins, B. Clennell, D. Dewhurst, and G. Westbrook (1994), Heterogeneous hydrofracture development and accretionary fault dynamics, *Geology*, *22*, 259–262.

Burst, J. F. (1969), Diagenesis of gulf coast clayey sediments and its possible relation to petroleum migration, *Bull. Am. Assoc. Pet. Geol.*, *53*, 73–93.

Carcione, J. M., H. B. Helle, N. H. Pham, and T. Toverud (2003), Pore pressure estimation in reservoir rocks from seismic reflection data, *Geophysics*, *68*, 1569–1579.

Cerney, B., and R. L. Carlson (1999), The effect of cracks on the seismic velocities of basalt from site 990, southeast Greenland margin, in *Proc. ODP, Scientific Results,* vol. 163, edited by H. C. Larsen et al., pp. 29–35, College Station (Ocean Drilling Program), Tex.

Cheng, C. H., and M. N. Toksoz (1979), Inversion of seismic velocities for the pore aspect ratio spectrum of a rock, *J. Geophys. Res.*, *84*, 7533–7543.

Christensen, N. I., and H. F. Wang (1985), The influence of pore pressure and confining pressure on dynamic elastic properties of Berea sandstone, *Geophysics*, *50*, 207–213.

Cleary, M. P., I. W. Chen, and S. M. Lee (1980), Self-consistent techniques for heterogeneous media, *Am. Soc. Civil Eng. J. Eng. Mech.*, *106*, 861–887.

Cochrane, G. R., J. C. Moore, M. E. MacKay, and G. F. Moore (1994), Velocity and inferred porosity model of the Oregon accretionary prism from multichannel seismic reflection data: Implications on sediment dewatering and overpressure, *J. Geophys. Res.*, *99*, 7033–7043.

Costa Pisani, P., M. Reshef, and G. Moore (2005), Targeted 3-D prestack depth imaging at Legs 190–196 ODP drill sites (Nankai Trough, Japan), *Geophys. Res. Lett.*, *32*, L20309, doi:10.1029/2005GL024191.

Crampin, S. (1985), Evaluation of anisotropy by shear wave splitting, *Geophysics*, *50*, 142–152.

Dahlen, F. A. (1984), Noncohesive critical Coulomb wedges: An exact solution, *J. Geophys. Res.*, *89*, 10,125–10,133.

Davis, D., J. Suppe, and F. A. Dahlen (1983), Mechanics of fold-and-thrust belts and accretionary wedges, *J. Geophys. Res.*, *88*, 1153–1172.

Dutta, N. C. (2001), Geopressure prediction using seismic data: Current status and the road ahead, *Geophysics*, *67*, 2012–2041.

Dvorkin, J., and A. Nur (1996), Elasticity of high-porosity sandstones: Theory for two North Sea data sets, *Geophysics*, *61*, 1363–1370.

Eaton, B. A. (1972), Graphical method predicts geopressures worldwide, *World Oil*, *182*, 6, 51–56.

Eberhart-Phillips, D., and D. Han (1989), Empirical relationships among seismic velocity, effective pressure, porosity and clay content in sandstone, *Geophysics*, *54*, 82–89.

Gamage, K., and E. Screaton (2006), Characterization of excess pore pressures at the toe of the Nankai accretionary complex, Ocean Drilling Program sites 1173, 1174, and 808: Results of one-dimensional modeling, *J. Geophys. Res.*, *111*, B04103, doi:10.1029/2004JB003572.

Han, D., and A. Nur (1986), Effects of porosity and clay content on wave velocities in sandstones, *Geophysics*, *51*, 2093–2107.

Hayward, N., G. K. Westbrook, and S. Peacock (2003), Seismic velocity, anisotropy, and fluid pressure in the Barbados accretionary wedge from an offset vertical seismic profile with seabed sources, *J. Geophys. Res.*, *108*(B11), 2515, doi:10.1029/2001JB001638.

Hill, R. (1952), The elastic behavior of a crystalline aggregate, *Proc. Phys. Soc. London A*, 65, 349–354.

Hoffman, N. W., and H. J. Tobin (2004), An empirical relationship between velocity and porosity for underthrust sediments in the Nankai Trough accretionary prism, in *Proc. ODP, Sci. Results*, vol. 190/196, edited by H. Mikada et al., pp. 1–23, College Station, Tex.

Hubbert, M. K., and W. W. Rubey (1959), Role of fluid pressure in mechanics of overthrust faulting, *Geol. Soc. Am. Bull.*, *70*, 115–166.

Hudson, J. A. (1981), Wave speeds and attenuation of elastic waves in material containing cracks, *Geophys. J. R. Astron. Soc.*, *64*, 133–150.

Hyndman, R. D., G. F. Moore, and K. Moran (1993), Velocity, porosity, and pore-fluid loss from the Nankai subduction zone accretionary prism, in *Proc. ODP, Sci. Results,* vol. 131, edited by I. A. Hill et al., pp. 211–220, College Station (Ocean Drilling Program), Tex.

Ienaga, M. (2003), The early stages of formation and evolution of the Nankai accretionary prism inferred from quantitative analysis of logging-while-drilling and core data, ODP Leg 196, Ph.D. thesis, Univ. of Tokyo, Japan.

Ienaga, M., L. C. McNeill, H. Mikada, S. Saito, D. Goldberg, and J. C. Moore (2006), Borehole image analysis of the Nankai accretionary wedge, ODP Leg 196: Structural and stress studies, *Tectonophysics*, *426*, 207–220.

Ito, T., S. Yoshioka, and S. Miyazaki (1999), Interplate coupling in southwest Japan deduced from inversion analysis of GPS data, *Phys. Earth Planet. Inter.*, *115*, 17–34.

Jakobsen, M., J. Hudson, T. Minshull, and C. Singh (2000), Elastic properties of hydrate-bearing sediments using effective medium theory, *J. Geophys. Res.*, *105*, 561–577.

Karig, D. E. (1993), Reconsolidation tests and sonic velocity measurements of clay-rich sediments from the Nankai Trough, in *Proc. ODP, Sci Results*, vol. 131, edited by I. A. Hill et al., pp. 247–260, College Station (Ocean Drilling Program), Tex.

Kondo, H., G. Kimura, H. Masago, K. Ohmori-Ikehara, Y. Kitamura, E. Ikesawa, A. Sakaguchi, A. Yamaguchi, and S. Okamoto (2005), Deformation and fluid flow of a major out-of-sequence thrust located at seismogenic depth in an accretionary complex: Nobeoka Thrust in the Shimanto Belt, Kyusyu, Japan, *Tectonics*, *24*, TC6008, doi:10.1029/2004TC001655.

Kuster, G. T., and M. N. Toksoz (1974), Velocity and attenuation of seismic waves in two-phase media, part 1—Theoretical formulations, *Geophysics*, *39*, 587–606.

Mavko, G., T. Mukerji, and J. Dvorkin (1998), *The Rock Physics Handbook, Tool for Seismic Analysis in Porous Media*, Cambridge Univ. Press, U.K.

McNeill, L. C., M. Ienaga, H. Tobin, S. Saito, D. Goldberg, J. C. Moore, and H. Mikada (2004), Deformation and in situ stress in the Nankai accretionary prism from resistivity-at-bit images, ODP Leg 196, *Geophys. Res. Lett.*, *31*, L02602, doi:10.1029/2003GL018799.

Mikada, H., et al. (2002), *Proc. ODP, Init. Repts., 196* [CD-ROM], available from: Ocean Drilling Program, Texas A&M Univ., College Station, Tex.

Mindlin, R. D. (1949), Compliance of elastic bodies in contact, *J. Appl. Mech.*, *16*, 259–268.

Miyazaki, S., and K. Heki (2001), Crustal velocity field of southwest Japan: Subduction and arc–arc collision, *J. Geophys. Res.*, *106*, 4305–4326.

Moore, G. F., and T. H. Shipley (1993), Character of the décollement in the Leg 131 area, Nankai Trough, in *Proc. ODP, Sci. Results*, vol. 131, edited by I. A. Fill et al., pp. 73–82, College Station (Ocean Drilling Program), Tex.

Moore, J. C., and H. Tobin (1997), Estimated fluid pressures of the Barbados accretionary prism and adjacent sediments, in *Proc. ODP, Sci. Results*, vol. 156, edited by T. H. Shipley et al., pp. 229–238, College Station, Tex.

Moore, J. C., and D. M. Saffer (2001), Updip limit of the seismogenic zone beneath the accretionary prism of southwest Japan: An effect of diagenetic to low-grade metamorphic processes and increasing effective stress, *Geology*, *29*, 183–186.

Moore, G. F., T. H. Shipley, P. L. Stoffa, D. E. Karig, A. Taira, S. Kuramoto, H. Tokuyama, and K. Suyehiro (1990), Structure of the Nankai Trough accretionary zone from multichannel seismic reflection data, *J. Geophys. Res.*, *95*, 8753–8765.

Moore, J. C., et al. (1998), Consolidation patterns during initiation and evolution of a plate-boundary décollement zone: Northern Barbados accretionary prism, *Geology*, *26*, 811–814.

Moore, G. F., et al. (2001a), Data report: Structural setting of the Leg 190 Muroto transect, in *Proc. ODP, Init. Repts.*, vol. 190, edited by G. F. Moore et al., pp. 1–14 [CD-ROM], Ocean Drilling Program, Texas A&M Univ., College Station, Tex.

Moore, G. F., et al. (2001b), New insights into deformation and fluid flow processes in the Nankai Trough accretionary prism: Results of Ocean Drilling Program Leg 190, *Geochem. Geophys. Geosyst.*, *2*(10), 1058, doi:10.1029/2001GC000166.

Moran, K., W. Bruckmann, V. Feeser, and R. G. Campanella (1993), In situ stress conditions at Nankai Trough Site 808, in *Proc. ODP, Sci. Results*, vol. 131, edited by I. A. Fill et al., pp. 283–291, College Station (Ocean Drilling Program), Tex.

Morgan, J. K., E. B. Ramsey, and M. V. S. Ask (2007), Deformation and mechanical strength of sediments at the Nankai subduction zone, in *The Seismogenic Zone of Subduction Thrust Faults*, edited by T. H. Dixon and J. C. Moore, pp. 210–256, Columbia Press, New York.

Norris, A. N. (1985), A differential scheme for the effective moduli of composites, *Mech. Mater.*, *4*, 1–16.

O'Connell, R. J., and B. Budiansky (1974), Seismic velocities in dry and saturated cracked solids, *J. Geophys. Res.*, *79*, 5412–5426.

Okamoto, S., G. Kimura, S. Takizawa, and H. Yamaguchi (2006), Earthquake fault rock indicating a coupled lubrication mechanism, *e-Earth*, *1*, 23–28.

Okino, K., Y. Ohara, S. Kasuga, and Y. Kato (1999), The Philippine Sea: New survey results reveal the structure and the history of the marginal basins, *Geophys. Res. Lett.*, *26*, 2287–2290.

Peacock, S. (2003), Thin layer tuned reflections from an anisotropic décollement zone, *J. Geophys. Res.*, *108*(B11), 2518, doi:10.1029/2001JB000195.

Powers, M. C. (1959), Adjustment of clays to chemical charge and the concept of the equivalence level, in *Clays Clay Miner.*, vol. 2, pp. 309–326, Pergamon Press, New York.

Rubey, W. W., and M. K. Hubbert (1959), Overthrust belt in geosynclinal area of western Wyoming in light of fluid pressure hypothesis, 2: Role of fluid pressure in mechanics of overthrust faulting, *Geol. Soc. Am. Bull.*, *70*, 167–206.

Saffer, D. M. (2003), Pore pressure development and progressive dewatering in underthrust sediments at the Costa Rican subduction margin: Comparison with northern Barbados and Nankai, *J. Geophys. Res.*, *108*(B5), 2261, doi:10.1029/2002JB001787.

Saffer, D. M. (2007), Pore pressure within underthrust sediment in subduction zones, in *The Seismogenic Zone of Subduction Thrust Faults*, edited by T. H. Dixon and J. C. Moore, pp. 171–209, Columbia Press, New York.

Saffer, D. M., and B. A. Bekins (1998), Episodic fluid flow in the Nankai accretionary complex: Timescale, geochemistry, flow rates, and fluid budget, *J. Geophys. Res.*, *103*, 30,351–30,370.

Sayers, C. M., G. M. Johnson, and G. Denyer (2002), Predrill pore pressure prediction using seismic data, *Geophysics*, *67*, 1286–1292.

Scholz, C. H. (1998), Earthquakes and friction lows, *Nature*, *391*, 37–42.

Schon, J. H. (2004), *Physical Properties of Rocks: Fundamentals and Principles of Petrophysics*, vol. 18, Elsevier, New York.

Screaton, E., D. Saffer, P. Henry, S. Hunze, and Leg 190 Shipboard Scientific Party (2002), Porosity loss within the underthrust sediments of the Nankai accretionary complex: Implications for overpressure, *Geology*, *30*, 19–22.

Seno, T., S. Stein, and A. E. Gripp (1993), A model for the motion of the Philippine Sea plate consistent with NUVEL-1 and geological data, *J. Geophys. Res.*, *98*, 17,941–17,948.

Shi, Y., and C. Y. Wang (1988), Generation of high pore pressures in accretionary prisms: Inferences from the Barbados subduction complex, *J. Geophys. Res.*, *93*, 8893–8910.

Shipboard Scientific Party (2001a), 4. Site 1173, in *Proc. ODP, Init. Repts.*, vol. 190, edited by G. F. Moore et al., pp. 1–147 [CD-ROM], Ocean Drilling Program, Texas A&M Univ., College Station, Tex.

Shipboard Scientific Party (2001b), 5. Site 1174, in *Proc. ODP, Init. Repts.*, vol. 190, edited by G. F. Moore et al., pp. 1–149 [CD-ROM], Ocean Drilling Program, Texas A&M Univ., College Station, Tex.

Shipley, T. H., G. F. Moore, N. L. Bangs, J. C. Moore, and P. L. Stoffa (1994), Seismically inferred dilatancy distribution, northern Barbados Ridge décollement: Implications for fluid migration and fault strength, *Geology*, *22*, 411–414.

Spinelli, G. A., P. S. Mozley, H. J. Tobin, M. B. Underwood, N. W. Hoffman, and G. M. Bellew (2007), Diagenesis, sediment strength, and pore collapse in sediment approaching the Nankai Trough subduction zone, *GSA Bull.*, *119*, 377–390.

Steurer, J. F., and M. B. Underwood (2003), Data report: The relation between physical properties and grainsize variations in hemipelagic sediments from Nankai Trough, in *Proc. ODP, Sci. Results*, vol. 190/196, edited by H. Mikada et al., pp. 1–25, College Station, Tex.

Straub, K. M. (2002), Fluid pressures in the Nankai Accretionary Prism: Ocean Drilling Program Sites 808, 1173, 1174, and 1177, Bachelor of Sci. in Geosci., Pennsylvania State Univ.

Swarbrick, R. E., and M. J. Osborne (1998), Mechanisms that generate abnormal pressures: An overview, in *Abnormal Pressures in Hydrocarbon Environments*, edited by B. E. Law, G. F. Ulmishek, and V. I. Slavin, *AAPG Mem.*, *70*, 13–34.

Taira, A., et al. (1991), Proceedings of the Ocean Drilling Program, *Initial Rep., 131*, Ocean Drill. Program, College Station, Tex.

Takahashi, N., S. Kodaira, A. Nakanishi, J. Park, S. Miura, T. Tsuru, Y. Kaneda, K. Suyehiro, and H. Kinoshita (2002), Seismic structure of western end of the Nankai trough seismogenic zone, *J. Geophys. Res.*, *107*(B10), 2212, doi:10.1029/2000JB000121.

Tobin, H., and D. Saffer (2003), Fluid pressure in the shallow plate interface at the Nankai Trough subduction zone, *Eos Trans. AGU*, *84*(46), Fall Meet. Suppl., Abstract T41A-04.

Tobin, H. D., P. Vannucchi, and M. Meschede (2001), Structure, inferred mechanical properties, and implications for fluid transport in the décollement zone, Costa Rica convergent margin, *Geology*, *29*, 907–910.

Toksoz, M. N., C. H. Cheng, and A. Timur (1976), Velocity of seismic waves in porous rocks, *Geophysics*, *41*, 621–645.

Tsuji, T., and G. J. Iturrino (2008), Velocity–porosity relationships of oceanic basalt from eastern flank of the Juan de Fuca ridge: The effect of crack closure on seismic velocity, *Exp. Geophys.*, *39*, 41–51.

Tsuji, T., T. Matsuoka, Y. Yamada, Y. Nakamura, J. Ashi, H. Tokuyama, S. Kuramoto, and N. Bangs (2005a), Initiation of plate boundary slip in the Nankai Trough off the Muroto peninsula, southwest Japan, *Geophys. Res. Lett.*, *32*, L12306, doi:10.1029/2004GL021861.

Tsuji, T., T. Noguchi, H. Niino, T. Matsuoka, Y. Nakamura, H. Tokuyama, S. Kuramoto, and N. Bangs (2005b), Two-dimensional mapping of finestructures in the Kuroshio Current using seismic reflection data, *Geophys. Res. Lett.*, *32*, L14609, doi:10.1029/2005GL023095.

Tsuji, T., G. Kimura, S. Okamoto, F. Kono, H. Mochinaga, T. Saeki, and H. Tokuyama (2006), Modern and ancient seismogenic out-of-sequence thrusts in the Nankai accretionary prism: Comparison of laboratory-derived physical properties and seismic reflection data, *Geophys. Res. Lett.*, *33*, L18309, doi:10.1029/2006GL027025.

Ujiie, K., T. Hisamitsu, and A. Taira (2003), Deformation and fluid pressure variation during initiation and evolution of the plate boundary décollement zone in the Nankai accretionary prism, *J. Geophys. Res.*, *108*(B8), 2398, doi:10.1029/2002JB002314.

Underwood, M. B., D. Saffer, K. Brown, J. Weinberger, K. Hoke, and J. Steurer (2001), sedimentary inputs into the Nankai seismogenic zone, *Eos Trans. AGU*, *82*(47), Fall Meet. Suppl., Abstract T51G-03.

Ursenbach, C. P. (2001), Simulation of elastic moduli of porous media, in *Extended Abstract of 71st Annual International SEG Meetings*, 1704–1707.

von Huene, R., and H. Lee (1982), The possible significance of pore fluid pressures in subduction zones, in *Studies in Continental Margin Geology*, edited by J. S. Watkins and C. L. Drake, *AAPG. Mem.*, *34*, 781–791, American Association of Petroleum Geologists (AAPG).

Westbrook, G. K. (1991), Geophysical evidence for the role of fluids in accretionary wedge tectonics, *Philos. Trans. R. Soc. London, Ser. A*, *335*, 227–242.

Xu, S., and R. E. White (1995), A new velocity model for clay–sand mixtures, *Geophys. Prospect.*, *43*, 91–118.

Yamano, M., M. Kinoshita, S. Goto, and O. Matsubayashi (2003), Extremely high heat flow anomaly in the middle part of the Nankai Trough, *Phys. Chem. Earth, [Solid Earth Geod.]*, *28*, 487–497.

Yilmaz, O., and S. Doherty (Eds.) (2001), *Seismic Data Processing*, 2nd ed., Invest. in Geophys., SEG, Tulsa, Okla.

Zhao, Z., G. F. Moore, N. L. Bangs, and T. H. Shipley (2000), Spatial variations of the décollement/protodécollement zone and their implication: A 3D seismic inversion study of the northern Barbados accretionary prism, *Island Arc*, *9*, 219–236.

Zhang, J. J., and L. R. Bentley (2003), Pore geometry and elastic moduli in sandstones, in *Expanded Abstract of 73rd Annual International SEG Meetings*, 5012–5015.

P. Costa Pisani, Customer Support Asia-Pacific, Paradigm Geophysical, Level 8, 256 St. Georges Terrace, Perth, WA 6000, Australia.

G. Moore, Department of Geology and Geophysics, University of Hawaii, 1680 East-West Road, POST 813 Honolulu, HI 96822, USA.

H. Tokuyama, Ocean Research Institute, University of Tokyo, 1-15-1, Minamidai, Nakano, Tokyo 164-8639, Japan.

T. Tsuji, Department of Civil and Earth Resources Engineering, Kyoto University, Katsura Campus, Nishikyo-ku, Kyoto 615-8540, Japan. (tsuji@earth.kumst.kyoto-u.ac.jp)